International Journal of Fatigue 171 (2023) 107564

Contents lists available at ScienceDirect

International Journal of Fatigue

journal homepage: www.elsevier.com/locate/ijfatigue

Codes and standards for the fatigue-based design of hydrogen infrastructure components

Carl Fischer [a,*], Sascha Fliegener [a], Heiner Oesterlin [a], Thorsten Michler [a], Susanne Höhler [b], Andreas Mondry [b], Pierre Ertault de la Bretonniere [a]

[a] Fraunhofer Institute for Mechanics of Materials IWM, Freiburg, Germany
[b] Salzgitter Mannesmann Forschung GmbH, Duisburg, Germany

ARTICLE INFO

Keywords:
Hydrogen infrastructure
Hydrogen transport
Hydrogen storage
Pressure vessel and pipeline steels
Codes and standards

ABSTRACT

A successful transition to a hydrogen economy and infrastructure requires robust engineering design codes. For the assessment of existing pipelines to be re-qualified from natural gas to hydrogen transport, the fracture mechanics design approach of the ASME B31.12 (2019) is often adapted to other national and regional standards. Several options to reduce the conservatism of the current version of the ASME B31.12 code are proposed. For the new design of storage tanks and other components, a fatigue-based approach should also be considered for the assessment of the influence of gaseous hydrogen. The German AD 2000 code proposes a methodology based on a fatigue life approach. Also here, options to reduce the conservatism of the current version are proposed. In addition, the German FKM guidelines provide a framework for additional design options. Both are subject to current developments. All relevant material test methods to measure mechanical properties of structural alloys in high pressure gaseous hydrogen are specified in ANSI/CSA CHMC 1. However, it is proposed to harmonize the detailed test conditions with other existing test standards, e.g. ASTM G142 or ISO 11114-4.

1. Introduction

A precondition for the upcoming hydrogen economy and infrastructure is a safe and reliable operation of the components in contact with hydrogen, e.g. pipelines, valves, fittings, compressors, tanks, turbines, etc. It is well known for over a decade that hydrogen deteriorates the mechanical properties of most structural alloys, especially steels. This phenomenon is often designated as “hydrogen embrittlement” (HE) and has a direct impact on the lifetime of hydrogen wetted components.

Intensive research focused on the underlying mechanisms of HE and several theories were proposed [1], among which the Hydrogen Enhanced Decohesion (HEDE) [2] and Hydrogen Enhanced Localized Plasticity (HELP) [3] appear to be the most plausible. The different proposed mechanisms clearly show that the nature of HE has not been understood in detail yet and intensive research is still ongoing. Furthermore, the proposed mechanisms are very complex and often operate on a micro scale or even atomic scale. That is, it seems unlikely that such mechanisms can be implemented in engineering design codes to account for hydrogen effects in the design process of engineering components.

A successful transition to a hydrogen economy and infrastructure requires robust engineering design codes that allow the safe and reliable design of hydrogen wetted components. Current benchmarks are the ASME B31.12 in combination with the ASME Boiler and Pressure Vessel Code - Section VIII - Div. 3 (2021), which specify the design of hydrogen pipelines and pressure vessels based on a fracture mechanics approach. Due to this fracture mechanics design approach, the application of the ASME codes is difficult to transfer to other components with thin wall thicknesses. Unfortunately, design codes that account for HE effects in the design of other hydrogen components (e.g. valves, fittings, compressors, etc.) are currently largely missing or in the early development stage, which is a severe obstacle for a fast upscaling of the hydrogen infrastructure.

The motivation of this study was to analyze the current benchmark design codes, i.e. ASME B31.12 in combination with the ASME Boiler and Pressure Vessel Code - Section VIII - Div. 3 especially in terms of design conservatism and to propose options to reduce the conservatism. For the design of other hydrogen components, the German AD 2000 code and the German FKM guidelines are analyzed, and it appears that both codes provide a solid framework to implement hydrogen effects in the design process. Finally, the very few available materials test

* Corresponding author.
E-mail address: carl.fischer@iwm.fraunhofer.de (C. Fischer).

https://doi.org/10.1016/j.ijfatigue.2023.107564
Received 1 December 2022; Received in revised form 3 January 2023; Accepted 6 February 2023
Available online 10 February 2023

Nomenclature

Symbols

a_1, a_2, a_3	Constants in ASME B31.12
a_0, a, a_{crit}	Initial, current, critical crack depth in ASME B31.12
a_{allow}	Allowable crack depth in ASME BPVC-VIII-3
a_{SK}	Load capacity in FKM guidelines
b_1, b_2, b_3	Constants in ASME B31.12
c_0	Half surface crack length $c_0 = l_0/2$
da/dN	Crack growth increment per loading cycle
$d\varepsilon/dt$	Strain rate in e.g. tensile tests
d_i	Inner diameter of e.g. pressure vessel
f	Cycle frequency in e.g. fatigue crack growth tests
f, f_{ref}	Fugacity at current pressure, reference fugacity of hydrogen
f_d, f_N, f_{T^*}	Reduction factors in AD 2000 bulletin S2 accounting for wall thickness, hydrogen and temperature effects
h	Triaxiality parameter in FKM guidelines
l, l_0, l_{crit}	Initial, current, critical surface crack length in ASME B31.12
m	Fatigue crack growth law exponent in BPVC Code Case 2938
p	Hydrogen pressure
p_{crit}	Load factor in FKM guidelines
p_{min}, p_{max}	Minimum, maximum hydrogen pressure in a loading cycle
r_i	Inner radius of e.g. pressure vessel
t	Wall thickness of e.g. pressure vessel
A, A_g	Tensile fracture strain, tensile uniform strain
$B1$	Constant in AD 2000 bulletin S2
C, C_H	Coefficients in BPVC Code Case 2938
F	Design factor in ASME B31.12
H_f	Hydrogen material performance factor in ASME B31.12
K	Stress intensity factor
K_{20}	Material strength coefficient at 20 °C in AD 2000 bulletin S2
K_{arrest}	Stress intensity factor at crack arrest
K_{IA}	Maximum applied stress intensity in ASME B31.12
K_{IAPP}	Applied stress intensity in e.g. ASME BPVC-VIII-3
K_{Ic}	Plane-strain fracture toughness in e.g. ASTM E399
K_{IH}	Threshold stress intensity factor in hydrogen in ASME B31.12
K_{IH}, K_{JH}, J_{IH}	Fracture toughness in hydrogen in e.g. ANSI/CSA CHMC 1
K_{min}, K_{max}	Minimum, maximum stress intensity factor in a loading cycle
N_{design}, N_{allow}, N_{crit}	Design, allowable, critical number of loading cycles in ASME B31.12 and ASME BPVC-VIII-3
N, N_{zul}, N^*_{zul}	Lifetime, acceptable lifetime, acceptable lifetime in gaseous hydrogen in AD 2000 bulletin S2
OD	Outer diameter of e.g. pressure vessel
R, R_σ	Load, stress ratio
RA	Reduction of area in tensile tests
R_m	Ultimate tensile strength in AD 2000 bulletin S2 and FKM guidelines
$R_{p0.2}$	0.2 % offset yield strength in AD 2000 bulletin S2 and FKM guidelines
β	Material-dependent property in FKM guidelines
Δa	Crack increment
ΔK	Stress intensity factor range
ΔK_{th}	Fatigue crack growth threshold
Δp	Pressure range
$\Delta\sigma_h$, $\Delta\sigma_r$	Hoop, radial stress range
ε_0	Minimum allowable strain in FKM guidelines
$\varepsilon_{pl,V}$	Maximum allowable equivalent plastic strain in FKM guidelines
$\varepsilon_{ref,1}$	True fracture strain at a stress triaxiality of $h = 0$ in FKM guidelines
σ_{min}, σ_{max}	Minimum, maximum stress in a loading cycle
σ_{UTS}	Ultimate tensile strength in ASME BPVC-VIII-3
σ_{YS}	Yield strength in ASME BPVC-VIII-3
$2\sigma_a$, $2\sigma^*_a$	Stress range, corrected stress range in AD 2000 bulletin S2
$2\sigma_{va}$	Maximum equivalent stress range in AD 2000 bulletin S2
$2\sigma_{zul}$	Maximum acceptable stress range in AD 2000 bulletin S2

Abbreviations

CT	Compact Tension
HAZ	Heat-Affected Zone
HE	Hydrogen Embrittlement
RNTS	Relative Notched Tensile Strength
RRA	Relative reduction of area
SF	Safety Factor
SYMS	Specified minimum yield strength in ASME B31.12
TMHE	Temperature of Maximum Hydrogen Embrittlement
UTS	Ultimate Tensile Strength

standards to measure mechanical properties in gaseous hydrogen atmosphere are compared to verify if the proposed test parameters are identical.

2. ASME B31.12 (2019)

The ASME B31.12 code is a worldwide accepted standard for the design and operation of pipelines for gaseous hydrogen and mixtures with more than 10 vol% of hydrogen and up to a maximum pressure of 21 MPa. The minimum temperature is limited to -62 °C. Steels according to standard API 5L PSL 2, i.e. X42 to X120 in R, N, Q or M conditions are recommended. The pipeline design pressure is calculated based on Barlow's formula depending on the nominal outer diameter and the wall thickness, a joint factor for the seam weld, the material yield strength and the operating temperature. Additionally, a design factor F and a hydrogen material performance factor H_f ensure a conservative assessment. The material performance factor is equal to unity for low–strength steels and low system design pressures, while $H_f < 1$ holds true for high yield strength steels and is monotonically decreased for pressures exceeding 1000 psig (about 6.9 MPa). The design factor F depends on the location of the pipeline e.g., on the number of buildings inhibited by humans in the surrounding area of the pipeline. A fracture mechanics assessment must be performed for pipeline integrity, if the hoop stress of the design pressure exceeds 40% of the materials specified minimum yield strength (SMYS). Therefore, two options are given for maximum design factors of 0.5 (option A) and 0.72 (option B). The Prescriptive Design Method (option A) for pipeline sizes larger than 114.3 mm (4.5 in.) includes three Charpy impact tests for each material heat according to the API 5L Annex G at zero degree Celsius or minimal operating temperature. The required minimum average shear values of the fracture appearance for different specimen types and minimum averaged Charpy impact energies are found in detail in chapter PL-3.7.1 of ASME B31.12. For welds, also three specimens from the weld material as well as from the heat affected zone are characterized in Charpy impact tests and have to guarantee specimen size–dependent Charpy impact energies. Annex G also specifies that the Charpy tests shall be performed "in the environment of pipeline application", which means that Charpy tests should be conducted in pressurized hydrogen gas. However, the authors are not aware of any existing test capabilities to perform such tests.

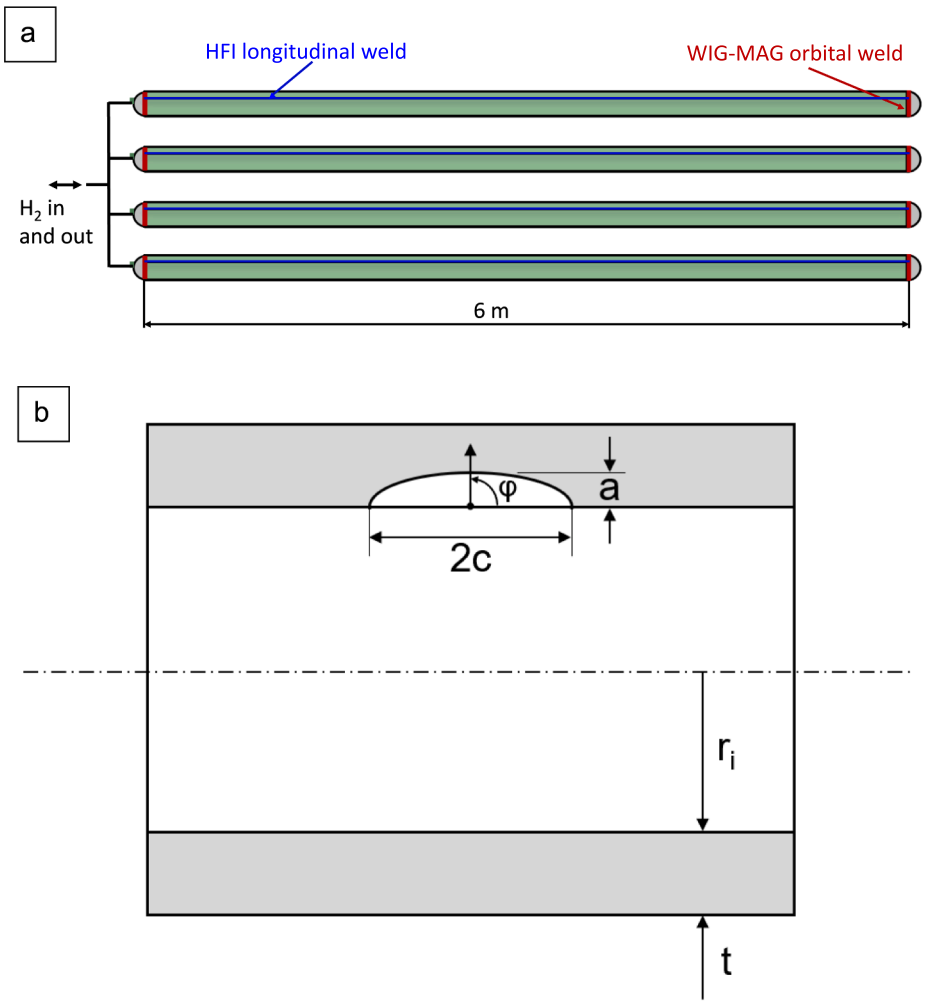

Fig. 1. a) Sketch of the tubular onshore hydrogen storage tank used as a use case. b) Axially-oriented semi-elliptical surface crack on the inner cylinder surface. Figure drawn according to API 579-1/ASME FFS-1 and adapted.

For a higher design factor F and a material performance factor of $H_f = 1$, the Performance–Based Design Method (option B) applies, which requires additional fracture mechanics testing in gaseous hydrogen atmosphere. The fracture mechanics testing program is based on the ASME Boiler and Pressure Vessel Code - Section VIII - Div. 3 (2021), herein abbreviated as ASME BPVC-VIII-3, in particular Article KD-10, which is described in detail later in Section 3.

For the fracture mechanics–based approach, an initial crack is assumed, which grows due to cyclic loading until the crack length reaches one of several lifetime criteria. The basis for the lifetime assessment is provided by fatigue crack growth curves and the fracture toughness, both measured in gaseous hydrogen atmosphere. An axially oriented, semi–elliptical crack on the inner surface of the pipeline is assumed, which is subjected to cyclic loading due to changes in the operating pressure. The crack geometry is schematically shown in Fig. 1. The initial crack size shall be determined by suitable non–destructive testing methods as described in ASME BPVC-VIII-3 Article KD-411. A depth-to-length aspect ratio of $a_0/l_0 = 1/3$ or $a_0/c_0 = 2/3$ is postulated. The maximum applied stress intensity K_{IA} along the crack front is obtained according to linear–elastic fracture mechanics solutions by means of the API 579-1/ASME FFS-1 (2016) manual. Alternative solutions are provided e.g., by the harmonized standard BS 7910 (2019).

The lifetime is obtained based on fatigue crack growth curves, which are experimentally determined for each material and material state as described in ASME BPVC-VIII-3 Article KD-10 (see Section 3). For this

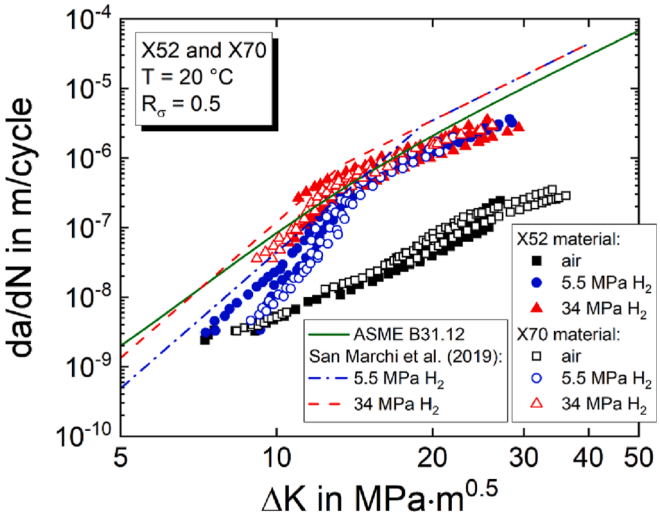

Fig. 2. Comparison of literature fatigue crack growth data with the predictions from the ASME B31.12 and from San Marchi et al. (2019) [8], including data for the pipeline steels X52 [6] and X70 [7] at different hydrogen gas pressures.

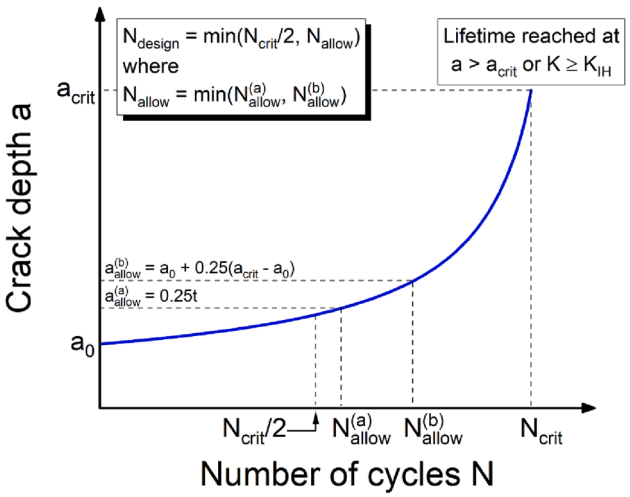

Fig. 3. Schematic crack growth evolution and determination of the design lifetime N_{design} according to ASME BPVC-VIII-3 Article KD-412.

reason, primarily fatigue crack growth data in gaseous hydrogen is published in literature for low alloy carbon pipeline steels, see e.g. [4,5]. Fig. 2 shows exemplary literature data from fatigue crack growth tests on compact tension (CT) specimens at different hydrogen gas pressures for two pipeline steels X52 and X70 [6,7]. The fatigue crack growth rates per loading cycle $\mathrm{d}a/\mathrm{d}N$ are plotted as a function of the stress intensity factor range $\Delta K = K_{max} - K_{min}$. For very low values of ΔK, the fatigue crack growth behavior in gaseous hydrogen seems to be unaffected and the crack growth rates are found close to those measured in laboratory air. However, crack growth in hydrogen is significantly accelerated around $\Delta K \approx 10\mathrm{MPa}\sqrt{\mathrm{m}}$. A stabilized behavior is reached for high driving forces at the crack tip, i.e. around $\Delta K \approx 15\mathrm{MPa}\sqrt{\mathrm{m}}$, and the slopes approximately equal those in ambient air. However, the crack growth rates in gaseous hydrogen are one to two orders of magnitude faster. The increase in hydrogen pressure from $p = 5.5$ MPa to $p = 34$ MPa tends only to slightly increase the crack growth rates. Although large differences in the crack growth behavior in air and hydrogen are apparent, only minor differences between the two pipeline steels with different material strengths are observed [7].

In case of no experimental data, a conservative enveloping design crack growth curve shown in Fig. 2 in dark green is alternatively given in ASME B31.12 (with reference to [4,5]), which approximates the experimentally observed crack growth behavior in gaseous hydrogen atmosphere by three power laws:

$$\frac{\mathrm{d}a}{\mathrm{d}N} = a_1 \Delta K^{b_1} + \left[\left(a_2 \Delta K^{b_2} \right)^{-1} + \left(a_3 \Delta K^{b_3} \right)^{-1} \right]^{-1}. \quad (1)$$

The constants are given in SI units to $a_1 = 4.0812 \cdot 10^{-9}$, $b_1 = 3.2106$, $a_2 = 4.0862 \cdot 10^{-11}$, $b_2 = 6.4822$, $a_3 = 4.881 \cdot 10^{-8}$ and $b_3 = 3.6147$ in Table PL-3.7.1-5. The application range of Eq. (1) is limited to a maximum hydrogen pressure of 20 MPa and a stress ratio of $R_\sigma = \sigma_{min}/\sigma_{max} \leq 0.5$. However, the application-specific hydrogen pressure and load ratio are not explicitly considered in Eq. (1). The phosphorous content of the pipeline material shall be less than 0.015 wt%, whereby the ultimate tensile strength of base and weld material shall be less than 758 MPa with a respective SMYS of less than 550 MPa. The design pressure is also limited to 85 % of the mill test pressure. Further limitations are given to the threshold stress intensity factor in hydrogen of $K_{IH} \geq 55\ \mathrm{MPa}\sqrt{\mathrm{m}}$, which shall be proven according to ASME BPVC-VIII-3 Article KD-10, see Section 3. This is also the upper value for K_{IA}, defining the critical number of cycles N_{crit}. Otherwise, N_{crit} is obtained, when the crack depth reaches a critical size a_{crit}, which is

- assumed in the ASME B31.12 as $a_{crit} = 0.25t$ with the wall thickness t and a critical surface crack length of $l_{crit} = 2c = 1.5t$ or
- determined according to Article KD-10 of ASME BPVC-VIII-3, which refers to Article KD-401(c) of ASME BPVC-VIII-3 and finally to the Level 2 or Level 3 failure assessment diagram (FAD) approach according to the API 579-1/ASME FFS-1 manual.

From safety reserve aspects, one of the two following options given in Article KD-412 of ASME BPVC-VIII-3 as shown in Fig. 3 hold true for the allowable crack size and the design lifetime N_{design}, which results in the lesser number of loading cycles:

- N_{design} is either half the number of cycles i.e., $N_{design} = N_{crit}/2$ (at a_{crit} or K_{IH}), where a_{crit} is determined according to Article KD-401(c) of ASME BPVC-VIII-3 and by means of the failure assessment diagram from API 579-1/ASME FFS-1 or
- N_{design} is the lesser number of loading cycles as obtained from Article KD-412(b) of ASME BPVC-VIII-3, where the allowable crack depth a_{allow} for monobloc vessels is limited to maximum 25 % of the considered thickness section ($N_{allow}^{(a)}$ at $a_{allow}^{(a)} = 0.25t$) as defined in Article KD-412.1(a) or when the crack has grown 25 % of the way from a_0 to a_{crit} i.e., $a_{allow}^{(b)} = a_0 + 0.25(a_{crit} - a_0)$ and $N_{crit}^{(b)}$ at $a_{allow}^{(b)}$, see Article KD-412.1(b) and finally $N_{allow} = \min\left(N_{allow}^{(a)}, N_{allow}^{(b)}\right)$.

For multilayer vessels, the reader is referred to ASME BPVC-VIII-3 Article KD-412.2.

3. ASME Boiler and Pressure Vessel Code - Section VIII - Div. 3 (2021)

The ASME BPVC - Section VIII - Div. 3 (ASME BPVC-VIII-3) standard covers alternative construction rules of high pressure vessels with given design pressures above 70 MPa. Article KD-10 accounts for pressure vessels in hydrogen applications. Special requirements must be fulfilled if the operating temperature of the pressure vessel is less than 95 °C and the hydrogen pressure is higher than 41 MPa for non-welded and higher than 17 MPa for welded vessels, respectively. For high strength materials with an ultimate tensile strength of $\sigma_{UTS} > 945$ MPa (for welds $\sigma_{UTS} > 620$ MPa), Article KD-10 applies already for hydrogen pressures exceeding 5.2 MPa. The requirements are non–mandatory for higher operating temperatures, however, temperature fluctuations due to start–up and shut–down cycles fall in the application range. For low alloy carbon steels, on which the focus is placed in this work, the maximum operating temperature is limited to 65 °C for hydrogen pressures higher than 100 MPa.

For each material condition and heat treatment, the threshold stress intensity factor in hydrogen K_{IH} shall be determined from the largest wall thickness. Three measurements in the final heat treatment condition must be carried out each for the base material, weld material and the heat affected zone (HAZ). Different welds of the vessel need to be recharacterized each for the weld material and the HAZ. The specimens should be extracted from the pipeline in TL direction (see e.g. ASTM E399 (2022) for more details). If this is not possible for the weld material and the HAZ, specimen extraction in LT direction is also allowed. However, the determined values apply also for similar materials from the same or similar specification or grade, chemical composition, heat treatment and material strength not exceeding the qualified values by 5 %. The lowest value for K_{IH} is used as a conservative reference in the fracture mechanics assessment. For the fatigue crack growth tests characterizing the hydrogen–induced fatigue crack growth behavior, the identical testing conditions and specimen orientations apply with the exception, that the specimens must not be extracted from the thickest section of the vessel. The highest measured crack growth rates (upper bound) are used for the following analysis.

The threshold stress intensity factor in hydrogen K_{IH} is determined according to the ASTM E1681 (2003) standard. Therefore, the specimen is pre-cracked in air by cyclic fatigue loading. Afterwards, the specimen is tested in a pressurized gaseous hydrogen environment at room temperature with impurity contents specified in ASME BPVC-VIII-3 Article KD-1046, which are typically ensured by using 99.9999 % (quality 6.0) hydrogen. Specimen loading is applied either by the constant load or constant displacement method. For the constant load test, a CT specimen geometry is commonly used and typically loaded by a weight or a servo–controlled actuator with a stress intensity of $K_{IAPP} > K_{IH}$, which is obtained from fracture mechanics calculations. A constant displacement (crack opening mouth displacement measured with a strain gauge) is realized by the use of modified bolt–load compact specimens, where the specimen is pre–strained to apply a stress intensity of $1.5K_{IH} < K_{IAPP} < 198\ \mathrm{MPa}\sqrt{\mathrm{m}}$. Suitable, yield strength-dependent K_{IAPP} starting values are specified in Article KD-1045, i.e. $159 - 198\ \mathrm{MPa}\sqrt{\mathrm{m}}$ for materials with a yield strength of $\sigma_{YS} \leq 621$ MPa.

From an experimental point of view, the constant displacement method is convenient to realize in autoclave test setups and, furthermore, multiple specimens can be tested simultaneously. For low alloy ferritic steels, the minimum test duration is 1000 h. Afterwards, the specimens are analyzed according to Article KD-1047 for subcritical crack growth. If the crack growth increment from the existing pre–fatigue crack is smaller than $\Delta a_{crit} < 0.25$ mm, the characterized material is qualified for the application in pressurized gaseous hydrogen components and it follows $K_{IH} = K_{IAPP}$ for the constant load and $K_{IH} = 0.5K_{IAPP}$ for the constant displacement method, respectively. Hence, for the required minimum threshold stress intensity of $K_{IH} > 55\ \mathrm{MPa}\sqrt{\mathrm{m}}$ in the ASME B31.12 standard, K_{IAPP} for the constant displacement method is often chosen to $K_{IAPP} = 110\ \mathrm{MPa}\sqrt{\mathrm{m}}$. In the case of $\Delta a_{crit} \geq 0.25$ mm, the applied stress intensity K_{IAPP} shall be adjusted appropriately that a crack arrest and, thus, subcritical crack growth is achieved during test duration, see ASTM E1681, which may involve retesting of a larger number of specimens. However, the candidate material is only characterized with regards to the minimum value of $K_{IH} > 55\ \mathrm{MPa}\sqrt{\mathrm{m}}$ as required in ASME B31.12, whereby the maximum fracture toughness is not exactly determined. An alternative procedure is given by Option B of the ISO 11114-4 (2017) standard, which is described in Section 8.3 in detail.

The obtained material parameters must fulfill a constraint validity check according to ASTM E1681. To ensure plain-strain conditions and linear elastic behavior, a minimum specimen thickness is required, which depends on the materials yield strength σ_{YS} and the determined K_{IH}. The yield strength is determined as an average value from three tensile specimens extracted adjacent to the fracture mechanics specimens in transverse orientation of the vesseland tested at room temperature according to ASTM SA-370 (2021). High values of the fracture toughness or K_{IH} in combination with low yield strengths result in larger specimen thicknesses, which exceed the typical wall thicknesses of pipelines and storage tanks. Hence, Article KD-10 also allows specimen testing with a thickness of greater than 85 % of the design wall thickness. However, the determined value for K_{IH} is solely valid for the characterized wall thickness. The transferability to other storage tank geometries and similar materials is not possible.

For the fracture mechanics assessment, also the plane-strain fracture toughness K_{Ic} is determined according to Article KM-250. The representative gaseous hydrogen conditions shall be identical to the subsequent fracture mechanics assessment. For a direct determination of the linear elastic, plane-strain fracture toughness K_{Ic}, ASTM E399 applies. In contrast to the K_{IH} tests, the specimens are monotonically loaded with a constant rate between $0.55\ \mathrm{MPa}\sqrt{\mathrm{m}}/\mathrm{s}$ and $2.75\ \mathrm{MPa}\sqrt{\mathrm{m}}/\mathrm{s}$ until the maximum force is reached before specimen fracture. Commonly used pipeline and storage tank materials exhibit often a ductile deformation behavior and the specimens are extracted from thin sections, so that the obtained values for K_{Ic} are not valid as required by ASTM E399. However, from *CTOD* or δ_{crit} (crack tip opening displacement) tests or *J*-integral fracture testing (J–R curve, *J*–integral evolution with the crack extension Δa) according to ASTM E1820 (2001) equivalent K_{Ic} values can be obtained by the conversion of the measured $K_{c\delta}$ or K_{JIc} values using the equations given in API 579-1/ASME FFS-1. In terms of gaseous hydrogen testing, the designation K_{JH} is also used for the fracture resistance, see e.g. [10]. The main benefits of this method are the determination of a representative material property and, the testing durations are significantly shorter compared to the characterization of the threshold stress intensity K_{IH} during 1000 h of hydrogen exposure in case of low alloy ferritic steels.

The fatigue crack growth behavior is determined in gaseous hydrogen conditions according to the ASTM E647 (2005) standard. Each material condition i.e., base material, weld material and HAZ is characterized by three crack growth curves. The load ratio is chosen as intended for component service. The test frequency is also adopted to the operation conditions, whereby the cycle frequency should not be faster than $f = 0.1$ Hz. The measured crack growth data in form of $\mathrm{d}a/\mathrm{d}N$–ΔK data pairs is used for the fracture mechanics analysis according to Article KD-4 or ASME B31.12 as described in Section 2.

4. German AD 2000 Code on Pressure Vessels (2018)

The German AD 2000 Code on Pressure Vessels (2018) contains all the essential safety requirements to be compliant with the European Pressure Equipment Directive (2014/68/EU). The series of EN 13445 (2021) standards, which cover unfired pressure vessels, are also based on the AD 2000 code. The normative technical bulletin S2 “analysis for cyclic loading” (2012) is relevant for the design and assessment of pressurized components in vessels, which are subjected to cyclic loading during operation due to internal pressures, temperature profiles or additional external forces. All AD 2000 documents are available in English language. In contrast to the ASME B31.12 and ASME BPVC-VIII-3 standards, the lifetime assessment is crack initiation-based on stress-life— (S–N) curves i.e., without the assumption of initial defects. Ferritic and austenitic, rolled and forged steels, spheroidal graphite cast iron materials, aluminum alloys as well as other wrought materials are included. In the following, the focus is placed on the ferritic steel materials for pipelines and pressure vessels.

For welded components, a structural stress analysis shall be performed either by experimental tests or by means of the finite element method, which gives the governing structural (or equivalent) stress distribution. The influence of notches is addressed separately in given S–N curves for welded joints. The stress determination of non-welded structures is obtained by a notch stress analysis, which is conducted e.g., with strain gauges placed in the notch or also by finite element calculations. Afterwards, the maximum decisive uniaxial or multiaxial equivalent stress range $2\sigma_{va}$ and, additionally for welds, the equivalent mean stress $\bar{\sigma}_V$, are calculated for the prevalent loading cycle defined by the mechanical and thermal loading histories under the assumption of Tresca’s maximum shear stress theory. For combined cyclic mechanical and thermal loadings exceeding the yield strength of the material ($\sigma_{va} > R_{p0.2/T^*}$), plastic strain concentration factors are introduced following the principle of the ASME BPVC - Section III - Div. 1 standard.

Two strategy options are given for the fatigue assessment of pressurized components in pressure vessels. The first option is to determine the maximum acceptable stress range $2\sigma_{zul}$ of the application in case of a targeted number of loading cycles. This approach distinguishes between non-welded structures and welded joints. For non–welded structures, the stress range $2\sigma_a$ is calculated with the targeted lifetime from tensile strength-dependent, design S–N curves for unnotched specimens and fully-reversed (i.e. without mean stress) loading conditions. The specified conservative lifetime curves were derived from experimental results and designed with safety factors based on statistical considerations about the lifetime scatter and failure probability. Alternatively, the

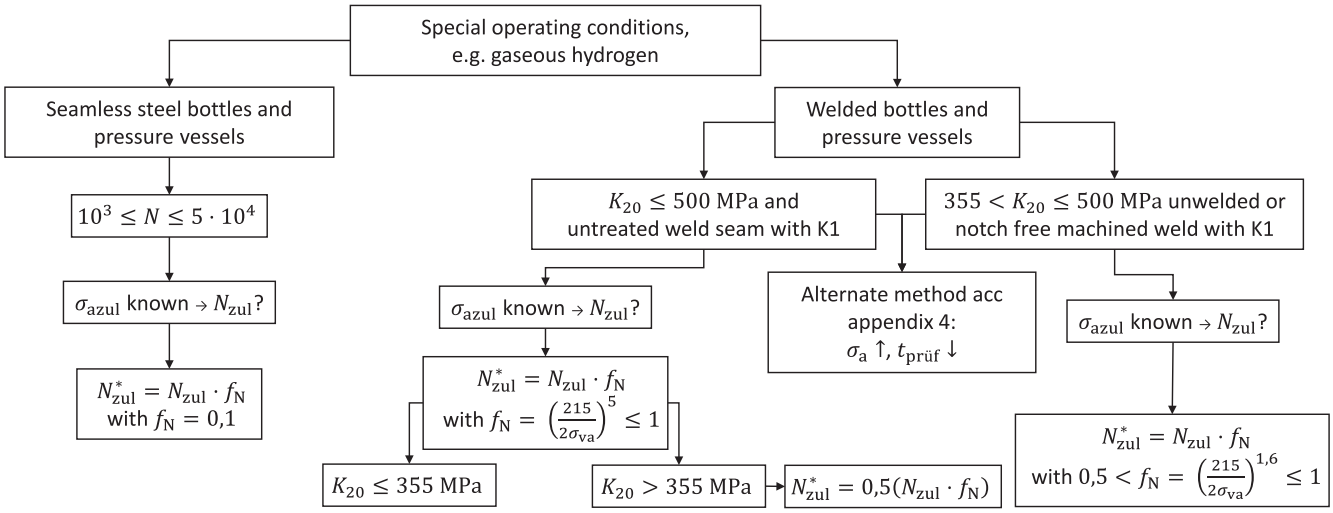

Fig. 4. Flow chart for a crack initiation–based lifetime assessment according to the AD 2000 bulletin S2.

stress range $2\sigma_a$ is obtained from a given empirical formula or for lifetimes above the fatigue endurance limit defined at $N \geq 2{\cdot}10^6$ cycles from tabulated values. The maximum acceptable stress range $2\sigma_{zul}$ is then obtained by the multiplication of the stress range $2\sigma_a$ with semi-empirical correction factors f accounting the surface roughness, wall thickness influence, mean stress effects and elevated temperatures.

A similar methodology is applied for welded joints. Here, the stress range $2\sigma_a$ is calculated depending on the weld seam finish. Typical weld joints for pressure vessels are divided in four classes (i.e. K 0 to K 3) on behalf of the notch effect. The differentiation in the respective weld classes requires a stress analysis, where additional stresses due to an offset in the wall thickness or due to the weld-on parts are considered (stress analysis option 1) or neglected (stress analysis option 2) in the foregoing structural stress analysis. Depending on the weld class, the stress range is gained from given lifetime curves for ferritic and austenitic rolled and forged steels, which were derived from stress- and strain-controlled fatigue tests on welded joint specimens. Alternatively, tabulated constants and an empirical formula are given for the calculation of the stress range $2\sigma_a$. Weld notch effects, residual stresses as well as the surface roughness and the mean stress influence are already considered in the design lifetime curves. Hence, only the correction factors for the temperature and the wall thickness are of further significance. Stress relief heat treatments have a positive effect on the residual weld stresses, the lifetime and, thus, on the acceptable stress range, which are accounted in the AD 2000 code by an additional correction factor $f \geq 1$ entering the mean stress influence.

The second option determines the allowable lifetime for a defined stress range obtained from the structural or notch stress analysis. For non-welded components, the lifetime is calculated with the correction factors accounting for influences due to the surface condition, wall thickness, mean stress and temperature as described previously. However, the load cycle-dependent correction factors accounting the surface roughness and wall thickness are found iteratively for the acceptable lifetime. For welded parts, the assessment is straight forward.

In the AD 2000, also an alternative calculation method for a higher acceptable number of load cycles is described, which are, however, coupled to shorter testing and maintenance periods. Load spectrums must be considered if the maximum stress range caused by the different operating loading types exceeds the fatigue endurance limit. Therefore, a linear damage accumulation hypothesis is applied.

The influence of gaseous hydrogen on the acceptable lifetime $N^*_{zul} = N{\cdot}f_N$ is considered with reduction factors f_N in dependence of existing weld seams, material strength and the weld seam quality itself, see Fig. 4. For steel cylinders and non-welded pressure vessels made of tempered steel (e.g. 34CrMo4), the hydrogen influence is taken into account by a reduction factor of $f_N = 0.1$ valid in a lifetime span between $10^3 \leq N \leq 5{\cdot}10^4$ cycles. As the respective experimental lifetimes (references are given in the AD 2000 code) were found slightly below the applied S–N curve for lifetime assessment, it was decided in the AD 2000 code to reasonably consider the influence of gaseous hydrogen with a "pragmatically" chosen reduction factor of $f_N = 0.1$, which corresponds to a failure probability of about 0.1 %. The lifetime assessment for welded pressure vessels of ferritic steels is possible up to a material strength coefficient of $K_{20} \leq 500$ MPa at 20 °C (i.e. interpreted as yield stress at room temperature) and non–finished weld seams. Here, the obtained lifetime from the second option is reduced for ferritic steels with $K_{20} \leq 355$ MPa by $f_N = \left(\frac{215}{2\sigma_{va}}\right)^5 \leq 1$ with $2\sigma_{va}$ being the equivalent stress range. Additionally, weld seam class K 1 (i.e. butt welds) is required. As mentioned in the explanations of bulletin S2, there is a lack of experimental fatigue data for welded fine-grained steel specimens in gaseous hydrogen atmosphere. Reference tests in air were found slightly above the respective design curve for weld class K 1. Hence, the reduction factor is substantiated with the experimental results in air and hydrogen, which fall in the lower scatter band of the experimental results for weld class K 1 and the "mean" lifetime curve exhibits a failure probability of less than 50 %, so that a safety factor 5 with the respect to the mean lifetime curve is found to be reasonable. The detrimental influence of hydrogen on the fatigue strength is considered upon a mean stress range of $2\sigma_{va} = 215$ MPa without further explanation. For higher strength ferritic steels with $K_{20} > 355$ MPa, the lifetime is additionally reduced to half of the calculated lifetime with the given reduction factors f_N. The rationale for this procedure is crack detection on hydrogen storage tanks and comparable weld specimens fatigue tests made of P355 and P460 steels, where the high strength steel showed a higher hydrogen sensitivity. The lifetime for ferritic steel pressure vessels with a material strength between $355 < K_{20} \leq 500$ MPa, which are non–welded or weld class K 1 is required and are finished notch–free, is assessed with a reduction factor of $f_N = \left(\frac{215}{2\sigma_{va}}\right)^{1.6} \leq 1$ and $f_N \geq 0.5$, since no significant differences are observed in the underlying experimental results between in air and in hydrogen atmosphere. For $K_{20} < 355$ MPa it follows $f_N = 1$, i.e. no detrimental influence of gaseous hydrogen on notch–free finished, weld class K 1 specimens is presumed, see Fig. 4.

5. European Industrial Gases Association - EIGA standards

The EIGA IGC Doc 121/14 (2014) for "Hydrogen Pipeline Systems" is

a detailed guideline for the safe design, operation and maintenance of metallic transport and distribution piping systems for pure hydrogen and hydrogen mixtures and is intended as a summary of current industrial practices and not understood as a mandatory standard. A wide temperature range between -40 °C and 175 °C and hydrogen pressures from 1 MPa up to 21 MPa are considered. The focus is also placed on the principal hazard and risk management of hydrogen operated pipelines due to the hydrogen damage mechanisms, e.g. HE and stress corrosion cracking. Candidate materials from different material classes, i.e. carbon steels, stainless steels, nickel, cobalt and copper alloys are specified. For the use of micro alloyed carbon steels in pressurized pure hydrogen pipelines, a maximum tensile strength of a X42/X52 grade according to API 5L PSL 2 is recommended. The maximum Rockwell hardness shall not exceed 95 HRB. The sulfur and phosphorus contents shall be less than 0.01 % and 0.015 %, respectively. A maximum carbon equivalent of 0.35 is specified. These specifications are all below the limits given in API 5L PSL 2.

For the qualification of the hydrogen influence on the material properties, EIGA IGC Doc 121/14 references to the relevant test methods such as ISO 11114-4 (see Section 8.3) and ASTM guidelines. For tensile tests on smooth as well as notched specimens, ASTM G142 shall be used, which is described in detail in Section 8.1. For evaluating the threshold stress intensity factor K_{IIH}, the reference is given to "various ASTM or ISO standards that can be modified for these tests". The anticipated standards are also covered in this paper. In addition, slow strain rate tests (SSRT) with a strain rate of approximately $d\varepsilon/dt = 10^{-7}/s$ (see ASTM G129) or disk pressure tests can be used for material qualification.

6. Use case "storage tank", comparison of design philosophies on design life prediction

In this section, a use case study is performed for a tubular onshore gaseous hydrogen storage tank consisting of multiple tubes with a length of 6 m (Fig. 1a). Based on the application as a high pressure hydrogen tank, AD 2000 S2 applies as the appropriate design code in Germany and Europe. However, due to the special design and the use of long pipes, the motivation was to verify if a design according to ASME B31.12 would result in more or less conservative dimensions knowing that ASME B31.12 is strictly not applicable for pressure vessel designs. For the assessment as a pipeline, a fracture mechanics-based lifetime assessment is performed according to the ASME B31.12 and ASME BPVC-VIII-3 codes described in Sections 2 and 3. For the assessment as a pressure vessel, the AD 2000 code from Section 4 results in a crack initiation-based lifetime prediction. In the following, the different design approaches from ASME B31.12 and AD 2000 codes for the lifetime prediction of the storage tank are compared and discussed. To this end, lifetimes are first predicted in Section 6.1 according to ASME B31.12 for different loading scenarios as well as varying initial crack sizes and aspect ratios. Furthermore, the influence of the underlying fatigue crack growth law and two different approaches for the stress intensity factor calculation are investigated. Afterwards, the lifetimes obtained by the ASME B31.12 design route are compared in Section 6.2 with the lifetimes obtained by the AD 2000 code. The considered storage tank for gaseous hydrogen is made of X52 API 5L low alloy carbon steel. The geometric dimensions provide an outer diameter of $OD = 2r_i + 2t = 323.9$ mm, a wall thickness of $t = 16$ mm, see Fig. 1b. The intended maximum pressure is limited to $p_{max} = 20$ MPa.

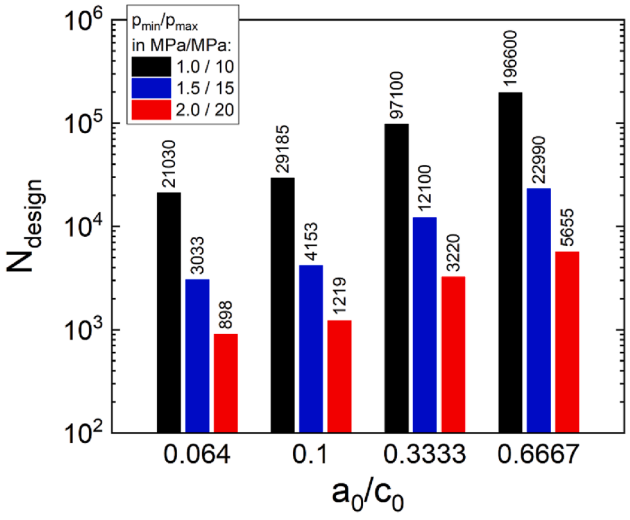

Fig. 5. Influence of the initial crack aspect ratio a_0/c_0 and the pressure level on the design lifetime N_{design} according to ASME B31.12 using the API 579-1/ASME FFS-1 stress intensity factor formulation for a constant initial crack depth of $a_0/t = 0.1$.

6.1. Fracture mechanics-based approach based on ASME B31.12

The expected crack geometry is the internal, semi-elliptical surface crack oriented in longitudinal direction of the storage tank, i.e. type KCSCLE1 in the API 579-1/ASME FFS-1 manual, which is subjected to internal pressure changes due to frequent filling and emptying cycles. The initial crack depth a_0 is not explicitly defined in the ASME B31.12 and shall be measured with suitable non-destructive testing methods. According to e.g. DIN EN ISO 10893-11 (2020), the initial crack depth is defined in different classes U2 to U5 between 5 % and 15 % of the wall thickness, which pipe manufactures have to verify, that the accuracy of the chosen ultrasonic testing method is capable to detect such a reference defect or notch with a respective specific size. Commonly, an initial crack depth of 10 % of the wall thickness according to class U3 is assumed. In this use case study, a crack depth of 5 % (class U2) is also supposed. Smaller initial crack depths e.g., 2.5 % of the wall thickness, are technically difficult to realize at the present time but are also considered in the following use case study to identify future potential for the design and lifetime calculations in case of small initial defect sizes. According to ASME BPVC-VIII-3 Article KD-10, an initial aspect ratio of $a_0/l_0 = 1/3$ ($a_0/c_0 = 2/3$) is assumed. A surface crack length of $l_0 = 50$ mm is suggested by the German technical rule DVGW G463:2021-10, which could be a defect along a pipe seam weld. Hence, different a_0/c_0 ratios are also considered in the following.

For the fracture mechanics and crack growth calculations, a workflow is implemented using the programming language *Python 3.7*. The stress intensity factor range ΔK is evaluated in surface direction ($\varphi = 0^\circ$) as well as in depth direction ($\varphi = 90^\circ$) of the crack using the functions and tabulated influence coefficients from API 579-1/ASME FFS-1 for the KCSCLE1 crack configuration, which includes crack face pressure loading. To this end, the influence coefficients are interpolated three-dimensionally for the current ratios of t/r_i, a/c and a/t. Therefore, the *RegularGridInterpolator* function from the *SciPy interpolate* bibliography is used. With the obtained ΔK values, the crack growth increments per loading cycle da/dN in case of the depth direction and $dl/dN = 2dc/dN$ in case of the surface direction are calculated by means of the given fatigue crack growth law in the ASME B31.12 or Eq. (1) and Fig. 2, respectively. The aspect ratio a/c is continuously updated. For the determination of the critical crack length a_{crit}, the Level 2 FAD approach from API 579-1/ASME FFS-1 is employed. The critical crack length is limited to the FAD curve or to 80 % of the wall thickness depending on which occurs first. The recommendations from ASME BPVC-VIII-3 Article KD-412.1 are applied for the design lifetime N_{design}, which are described in detail in Section 2 and are graphically shown in Fig. 3. In order to reduce the total calculation time integrating the crack growth increments for every single loading cycle, an integration scheme is implemented, where only the first four significant digits of the critical number of loading cycles N_{crit} are calculated. The maximum relative

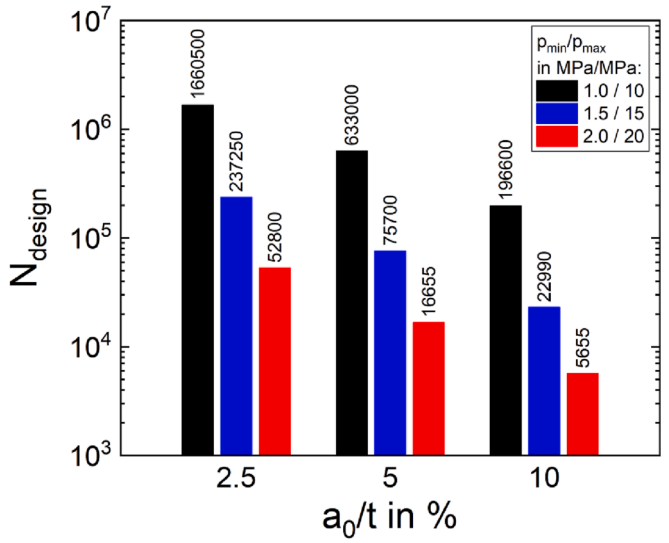

Fig. 6. Influence of the initial crack depth a_0 in relation to the wall thickness t and the pressure level on the design lifetime N_{design} according to ASME B31.12 using the API 579-1/ASME FFS-1 stress intensity factor formulation for a constant initial crack aspect ratio of $a_0/c_0 = 2/3$.

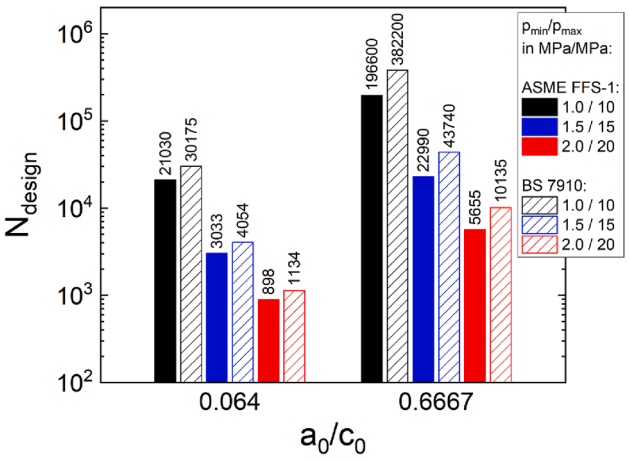

Fig. 7. Influence of the stress intensity factor solution from API 579-1/ASME FFS-1 and BS 7910 and the pressure level on the design lifetime N_{design} according to ASME B31.12 for two initial crack aspect ratios a_0/c_0 and a constant initial crack depth of $a_0/t = 0.1$.

error in relation to the considered exemplary exact results was found to be less than 0.3 % in lifetime and, thus, negligible.

Varying initial crack sizes and depths on the lifetime predictions are investigated in Sections 6.1.1 and 6.1.2. For exemplary lifetime predictions in Section 6.1.3, the influence of the underlying stress intensity factor solution is also calculated with the solution from BS 7910 for the "internal surface flaw in cylinder oriented axially", where crack face pressure loading is neglected. Here, the identical three dimensional interpolation scheme is applied. The influence of the assumed fatigue crack growth law is demonstrated in Section 6.1.4.

6.1.1. Influence of the initial crack aspect ratio

In the first lifetime predictions, the influence of the initial crack aspect ratio a_0/c_0 on the design lifetime is considered. While the initial crack depth a_0 is kept constant to 10 % of the wall thickness t, i.e. $a_0/t = 0.1$, the surface crack length c_0 is varied between 3.2 mm and 25 mm resulting in aspect ratios of $0.064 \leq a_0/c_0 \leq 2/3$. Maximum operating pressures of $p_{max} = 10$ MPa, 15 MPa and 20 MPa are considered for a constant load ratio of $R = p_{min}/p_{max} = 0.1$. The stress intensity factor is calculated according to API 579-1/ASME FFS-1 and the crack growth law from ASME B31.12 is applied.

The results are presented in Fig. 5, where the design lifetime is plotted as bar chart in logarithmic scale for the considered aspect ratios. The pressure level is highlighted by the color of the respective bar. For each loading scenario, the design lifetime is given in the diagram. Although the critical number of loading cycles N_{crit} is calculated for the first significant digits, it appears in some cases due to the division of N_{crit} by factor two, that five significant digits are obtained for N_{design}. The results in Fig. 5 clearly depict, that the lifetime of the storage tank is strongly dependent on the maximum applied hydrogen pressure level, where the lifetime is significantly reduced by a factor of about 6.9 to 8.6 increasing the maximum pressure from 10 MPa to 15 MPa and by a factor of 3.4 to 4.1 between 15 MPa and 20 MPa. In addition, a shorter initial surface crack length c_0 i.e., a larger aspect ratio a_0/c_0, leads to extended lifetimes. The assumption of a large initial surface crack length e.g., along the seam weld, of $l_0 = 2c_0 = 50$mm as suggested by the German technical rule DVGW G463:2021-10 results in conservative lifetime predictions. Higher design cycle numbers are obtained with the recommendations from ASME BPVC-VIII-3 Article KD-410 with a respective crack aspect ratio of $a_0/c_0 = 2/3$. Hence, for a maximum pressure of $p_{max} = 20$ MPa, the lifetime is increased by factor of about 6.3 assuming small surface crack lengths and an aspect ratio of $a_0/c_0 = 2/3$ instead of $a_0/c_0 = 0.064$.

6.1.2. Influence of the initial crack depth

In Fig. 6, the influence of the initial crack depth a_0 on the design lifetime N_{design} is investigated. Therefore, the ratio of a_0 to the wall thickness t is varied between $0.025 \leq a_0/t \leq 0.1$ for a load ratio of $R = 0.1$. The initial crack aspect ratio is constantly chosen as $a_0/c_0 = 2/3$. The stress intensity factor is calculated by means of API 579-1/ASME FFS-1 and the underlying crack growth law is taken from ASME B31.12. The shortest lifetimes are consequently obtained for an initial crack depth of $a_0/t = 0.1$. The operating pressure level has a pronounced influence on the resulting lifetime, which decreases by a factor up to 38 when the maximum pressure is doubled from $p_{max} = 10$ MPa to $p_{max} = 20$ MPa. If an initial crack depth of $a_0/t = 0.05$ can be ensured, the lifetime span is significantly enhanced in a range between factor 2.9 and 3.3 compared to $a_0/t = 0.1$. A further gain in lifetime would be possible if present defects can be detected with an accuracy of $a_0/t = 0.025$, which would result in a lifetime extension of factor 2.6 to 3.2 for the examples displayed in Fig. 6 in comparison to a starting crack length of $a_0/t = 0.05$. These observations are explained by the exponential fatigue crack growth behavior, as schematically shown in Fig. 3. Hence, a focus should be placed in the future on the more precise detection of defects by non-destructive testing methods for existing storage tanks and higher manufacturing standards for new designed storage tanks.

6.1.3. Influence of the stress intensity factor solution

In this subsection, the stress intensity factor solutions for the axially oriented, semi-elliptical surface crack on the inner surface of a cylinder (see Fig. 1b) from the harmonized standards API 579-1/ASME FFS-1 and BS 7910 are compared. Generally, the multidimensional and often highly non-linear stress distribution at the crack tip for various crack geometries is often determined by numerical simulation techniques e.g., by the finite element method. The obtained results for the membrane and bending stresses are then approximated by higher order, multidimensional polynomial functions using the weight function technique approach. In case of not fully analytical solutions, the coefficients, or influence coefficients as named in API 579-1/ASME FFS-1, are given as tabulated values for certain simulated data points (e.g. a/t or a/c ratios) and have to be interpolated (multidimensionally) to the current ratio of the considered variables.

The influence of the stress intensity factor solutions is investigated in Fig. 7 for two crack aspect ratios of $a_0/c_0 = 0.064$ and $a_0/c_0 = 2/3$ for an initial crack depth of $a_0/t = 0.1$. The crack growth law from ASME

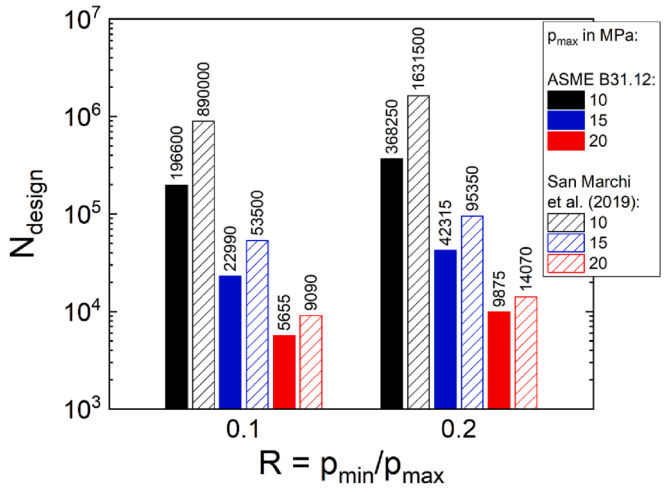

Fig. 8. Influence of the fatigue crack growth law from ASME B31.12 and San Marchi et al. [8] and the load ratio on the design lifetime N_{design} according to ASME B31.12 using the API 579-1/ASME FFS-1 stress intensity factor formulation for an initial crack aspect of $a_0/c_0 = 2/3$ and an initial crack depth of $a_0/t = 0.1$.

B31.12 is applied. The primary membrane stress P_m and primary bending stress P_b, which are necessary for the application of BS 7910, are calculated according to API 579-1/ASME FFS-1 with $P_m = pr_i/t$ and $P_b = p/2$. Misalignment and stress concentration factors as well as secondary membrane and bending stresses are assumed as zero. For the considered load scenarios and crack aspect ratios, the stress intensity factor solution from BS 7910 gives slightly non-conservative lifetimes with a factor of maximum 1.5 in case of $a_0/c_0 = 0.064$ and a factor of about 1.9 in case of $a_0/c_0 = 2/3$, respectively. The differences are addressed to the underlying polynomial order, the validity range (especially for the a/t or a/c ratios) and the consideration of crack face pressure, which is the case for API 579-1/ASME FFS-1 and not for BS 7910. With regards to a safe design and operation of hydrogen storage tanks, the stress intensity factor solution from API 579-1/ASME FFS-1 is used in the following calculations.

6.1.4. Influence of the fatigue crack growth law

In the ASME B31.12 standard, the conservative enveloping fatigue crack growth curve from Eq. (1) as shown in Fig. 2 is given, which can be used for the lifetime assessment, when no experimental data is available. Since the given fatigue crack growth formulation from Eq. (1) describes only the upper bound of experimental data, which results consequently in conservative lifetime predictions, the fatigue design curve from the BVPC Code Case 2938 for SA-372 and SA-723 pressure vessel and component steels was adapted by San Marchi et al. [8] also to low alloy ferritic pipelines steels. This design curve includes two characteristic crack growth regions for low $\Delta K < \Delta K_c$ and high $\Delta K \geq \Delta K_c$ regimes and covers the influence of the stress ratio and the hydrogen gas pressure. The knee point between both regimes is defined at the stress intensity ΔK_c, which is approximately obtained with $\Delta K_c = 8.475 + 4.062R_\sigma - 1.696R_\sigma^2$. To account for pressure effects on the fatigue crack growth rates of low alloy carbon pipeline steels, an additional fugacity f term was added, see [8]:

$$\frac{da}{dN} = C\left[\frac{1 + C_H R_\sigma}{1 - R_\sigma}\right]\Delta K^m \left(\frac{f}{f_{ref}}\right)^{0.5}. \quad (2)$$

The coefficients C, C_H and m are determined from curve fits and are given in [8] as follows: $C = 3.5{\cdot}10^{-14}$ m/cycle, $C_H = 0.4286$ and $m = 6.5$ for $\Delta K < \Delta K_c$, while $C = 1.5{\cdot}10^{-11}$ m/cycle, $C_H = 2.0$ and $m = 3.66$ for $\Delta K \geq \Delta K_c$. The pressure dependence in the low ΔK regime is described empirically with the square root of the fugacity term with f being the hydrogen fugacity at the current pressure and f_{ref} the hydrogen fugacity at a reference pressure, respectively. The square root dependency represents Siewerts law which appears to be a conservative assumption under the given operating conditions [9]. Eq. (2) applies for gaseous hydrogen pressures of $p \leq 103$ MPa, for materials with an ultimate tensile strength up to 915 MPa and up to maximum stress intensity factors of $K_{max} < 40$ MPa$\sqrt{m}$.

In Fig. 2, the crack growth law from San Marchi et al. [8] and Eq. (2) is shown for the two hydrogen pressures next to the experimental data. Please note, that the enveloping design curve from the ASME B31.12 is only applicable to a maximum pressure of $p \leq 20$ MPa. Especially in the lower and upper regimes of ΔK, the experimentally observed hydrogen assisted crack growth rates of the blue curves at 5.5 MPa pressure are significantly overestimated by the ASME B31.12 design curve, which results in conservative lifetime predictions. A more accurate description is achieved with the formulation from [8], where the different pressure levels are considered by the fugacity extension in Eq. (2). However, the crack growth behavior is still overestimated in the high ΔK regime and Eq. (2) is only valid up to $K_{max} < 40$ MPa$\sqrt{m}$, which is below the limit given in ASME B31.12 of $K_{IA} \leq K_{IH} = 55$ MPa$\sqrt{m}$.

The differences of both considered fatigue crack growth laws and of the load ratio R on the predicted design lifetime are investigated in Fig. 8. The starting crack geometry is $a_0/c_0 = 2/3$ and $a_0/t = 0.1$. Less conservative predictions are obtained using the fatigue crack growth law from San Marchi et al. [8] and Eq. (2), respectively. The influence is significantly pronounced for lower maximum pressures e.g., $p_{max} = 10$ MPa, since smaller fatigue crack growth rates are predicted in the ΔK regime up to $\Delta K \approx 15$ MPa$\sqrt{m}$, where crack growth takes place in a significant fraction of the total lifetime. For a load ratio of $R = 0.1$ and a maximum pressure of $p_{max} = 20$ MPa, the benefit in lifetime is found to be only around a factor of about 1.6. A higher load ratio of $R = 0.2$ leads generally to increased lifetimes due to smaller pressure fluctuations resulting in lower stress ranges. The identical trend is observed, that the crack growth law from [8] predicts a significant increase in N_{design} for minor operating pressures by a factor of about 4.4 at the lowest maximum pressure of 10 MPa, where a design lifetime of more than 1.6 million cycles is obtained for the hydrogen storage tank in this loading scenario.

6.2. Crack initiation-based approach based on the German AD 2000 code

This section focusses on the lifetime assessment with the crack initiation–based approach based on the AD 2000 code and comprises the results with the predictions obtained by the ASME B31.12. First, the application of the AD 2000 is described in detail.

Since the considered hydrogen storage tank consists of several welded short pipe segments, the assessment route in the AD 2000 code for welded pressure vessels is applied. All pipe segments exhibit a seam weld, whereby the caps exhibit a girth weld. Due to the occurrence of the highest stress i.e., the hoop stress, the seam weld is considered in the following lifetime predictions. The seam weld is manufactured by automatic high frequency induction (HFI) welding, whereby the upset metal is directly removed from both the inner and outer surfaces by chipping. In the AD 2000 code, this weld type is classified as class K 1.

For welded components, the acceptable lifetime N_{zul} in the AD 2000 bulletin S2 is determined as follows:

$$N_{zul} = \frac{B1}{\left(2\sigma_a^*\right)^3}. \quad (3)$$

The constant $B1$ holds $B1 = 5{\cdot}10^{11}$ cycles in case of weld class K 1 valid in a lifetime span of $10^2 \leq N \leq 2{\cdot}10^6$ cycles. The latter of the stress range $2\sigma_a^*$ is expressed as

$$2\sigma_a^* = \frac{2\sigma_{va}}{f_d f_{T^*}}, \quad (4)$$

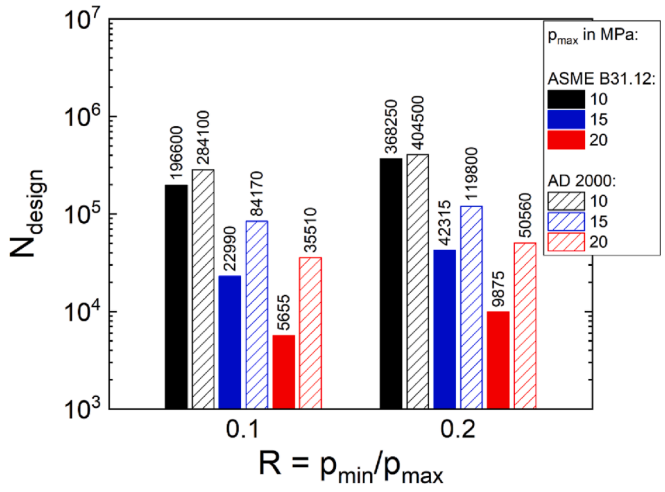

Fig. 9. Comparison of the design approaches from ASME B31.12 using the API 579-1/ASME FFS-1 stress intensity factor formulation for an initial crack aspect of $a_0/c_0 = 2/3$ and an initial crack depth of $a_0/t = 0.1$ and AD 2000 bulletin S2 on the design lifetime N_{design} for different pressure levels and load ratios.

where $2\sigma_{va}$ denotes the equivalent stress range following the maximum shear stress theory or Tresca's yield criterion. The reduction factor f_d accounts for wall thicknesses exceeding $t > 25$ mm and the reduction factor f_{T^*} for temperatures of $T^* > 100\ ^\circ$C, respectively. Hence, both reduction factors are reduced to unity. The equivalent stress range $2\sigma_{va}$ for the hydrogen storage tank is obtained from the largest difference of the maximum principal stress ranges, which are contributed for an internally pressurized cylinder vessel by the fractions of the circumferential or hoop stress σ_h and radial stress σ_r. Thus, the equivalent maximum principal stress range $2\sigma_{va}$ is written to

$$2\sigma_{va} = \Delta\sigma_h - \Delta\sigma_r. \tag{5}$$

Since fatigue crack initiation is primarily expected to occur at the inner surface of the storage tank, the hoop stress range $\Delta\sigma_h$ is determined at the inside diameter d_i using Lamé's equations with

$$\Delta\sigma_h = \frac{\Delta p d_i^2}{OD^2 - d_i^2}\left(1 + \frac{OD^2}{d_i^2}\right), \tag{6}$$

where $d_i = 2r_i$ and $OD = 2r_i + 2t$ following the dimensions introduced in Fig. 1 and $\Delta p = p_{max} - p_{min}$. Eq. (6) results consequently in slightly lower values than Barlow's formula given e.g., in ASME B31.12, where the outer diameter is taken into account for the hoop stress calculation. According to Lamé's theory, the inside radial stress range $\Delta\sigma_r$ is considered by

$$\Delta\sigma_r = -\Delta p = -(p_{max} - p_{min}). \tag{7}$$

The choice is also justified by the definition of a thick-walled cylinder according to ASME B31.8 (2020) for $OD/t < 30$, which is the case for the considered storage tank geometry with $OD/t = 323.9/16 \approx 20$. Due to the negative sign in Eq. (7), the radial component is added in Eq. (5) on the hoop stress component. With the determined equivalent maximum principal stress range $2\sigma_{va}$, the stress range $2\sigma_a^*$ is obtained by Eq. (4) and finally the acceptable lifetime N_{zul} according to Eq. (3). The number of loading cycles has to be interpreted as lifetime without consideration of the detrimental influence of gaseous hydrogen on the fatigue properties.

To this end, the reduction factor f_N has to be calculated, which is described in Section 4 in detail. Due to the weld seam surface finish by chipping but no notch-free grinding, the following reduction factor f_N holds true:

$$f_N = \left(\frac{215}{2\sigma_{va}}\right)^5 \leq 1. \tag{8}$$

The considered X52 low alloy carbon steel was characterized in tensile tests in laboratory air and in gaseour hydrogen in longitudinal as well as transverse direction of the pipe segment. The experimental material characterization results will be published separately. In both directions, the 0.2 % offset yield strength of the X52 material was found in a range of $R_{p0.2} = 455 \pm 2$ MPa in transversal and $R_{p0.2} = 475 \pm 7$ MPa in longitudinal orientation. Hence, the material strength coefficient is $K_{20} > 355$ MPa and, thus, the acceptable lifetime N_{zul}^* accounting gaseous hydrogen influence is:

$$N_{zul}^* = 0.5(N_{zul}\, f_N). \tag{9}$$

It is noted for the considered pressure scenarios, that $2\sigma_{va}$ is always lower than the limit of $2\sigma_{va} = 215$ MPa in Eq. (8), and thus, it holds $f_N = 1$. Hence, a safety factor of two is generally applied on the acceptable lifetime N_{zul}^*.

Fig. 9 shows the lifetime predictions obtained by the AD 2000 standard (dashed bars) and compares the results with the ASME B31.12, shown in solid bars. For the fracture mechanics-based lifetime assessment, a crack geometry of $a_0/c_0 = 2/3$ and $a_0/t = 0.1$ is assumed. The stress intensity factor is calculated by means of the API 579-1/ASME FFS-1 manual and the crack growth rates da/dN or dc/dN with the crack growth curve from the ASME B31.12, see Fig. 2. The acceptable lifetime N_{zul}^* from the AD 2000 code is also designated as N_{design} in Fig. 9. Less influence of the mechanical loading i.e., the maximum pressure, on the lifetime is observed for the crack initiation-based approach by the AD 2000. A higher load ratio results in prolonged lifetimes. For the lowest maximum pressure of $p_{max} = 10$ MPa, both design approaches predict quite similar lifetimes, the deviation is found only around a factor of 1.4 in favor of the AD 2000. However, the influence of the mechanical loading is significantly pronounced for the maximum pressures of $p_{max} = 15$ MPa and $p_{max} = 20$ MPa, where the lifetime predictions deviate in a range of about 2.8 to 3.7 ($p_{max} = 15$ MPa) and in a range of about 5.1 to 6.3 ($p_{max} = 20$ MPa), respectively. Hence, the assessment according to AD 2000 results in significantly less conservative lifetime predictions compared to the ASME B31.12 for high operating pressure levels.

This trend is explained by the different modeling concepts, where the AD 2000 considers the lifetime spent in the crack initiation and early crack growth phase up to a technical crack length of ca. 1 to 2 mm, while the ASME B31.12 assumes an initial defect in the length range of a technical crack ($a_0 = 1.6$ mm in case of $a_0/t = 0.1$) and describes the subsequent crack growth behavior until a certain lifetime criterion according to Fig. 3 is reached. The assumption of a pre–existing initial crack (e.g. material inhomogeneity) results a priori in conservative lifetime predictions. The deviation in the predicted lifetime between ASME B31.12 and AD 2000 standards is consequently decreased if a smaller initial defect size of $a_0/t = 0.05$ can be ensured and reliably detected with non-destructive testing methods for new hydrogen storage tanks and other components of the hydrogen infrastructure.

The strength of the AD 2000 code is the differentiation between non–welded and welded structures and the classification of the weld seam and surface finish. Load spectrums are also considered. Empirical equations and diagrams are given for the calculation of the allowable stress range or lifetime, so that own experimental tests do not necessarily have to be performed. The detrimental influence of gaseous hydrogen is taken into account with reduction factors. However, there are only two references mentioned in the AD 2000 code on which the assumptions and estimates regarding the hydrogen reduction factors are based on. This provides several opportunities to optimize the crack initiation criteria for hydrogen applications, e.g. the influence of the hydrogen gas pressure, the influence of the load cycle frequency and the load ratio, the influence of the microstructure morphology in terms of the weld seam

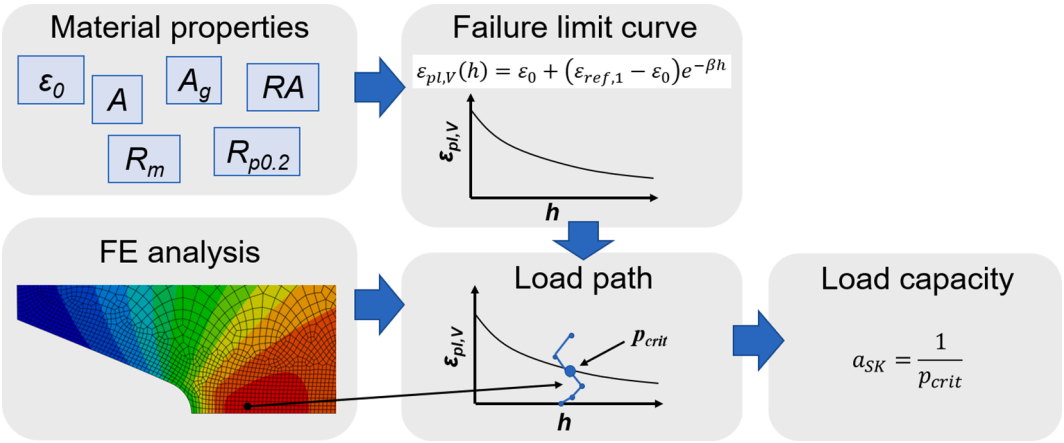

Fig. 10. Illustration of the strain-based nonlinear static strength justification scheme according to [12]. Based on material properties, the failure limit curve is derived, defining the maximum allowable equivalent strain dependent on the stress triaxiality. From FE analysis, the load factor p_{crit} is determined, defining the point of failure when the load path intersects with the failure limit curve. Finally, a load capacity of the component a_{SK} is derived. An example for a full data set is given in Table 1.

with base material, weld material and heat affected zones and the influence of the temperature (not relevant for pipeline periphery and storage tanks).

7. German FKM guidelines: Strength justification for engineering components

7.1. General overview

The German FKM guidelines [11–13] were published by the German research association mechanical engineering (FKM) [14] of the German Association for Mechanical and Plant Engineering (VDMA) [15] since 1994. Their development and further extension are continuously ongoing. The FKM guidelines represent analytical dimensioning schemes for a vast variety of structural components and have gained significant acceptance especially for small and medium enterprises (SME) in Germany. Due to their translation into English, the FKM guidelines are established in other European countries as well. They are applicable to a wide range of materials (steel, stainless steel, cast iron, aluminum, cast aluminum) and temperatures (e. g. -40 °C to 500 °C for steels) as well as for welded structures. The first guideline "Analytical strength justification for engineering components" [11] was first published in 1994 and provides a dimensioning scheme applicable to static and fatigue loading using nominal or local stresses, e.g. from finite element (FE) simulations. The parameters such as material properties are available in tabular form for different material classes, enabling a complete dimensioning process of a component without the necessity to measure material properties in experiments. Additionally, the guideline offers the possibility to estimate unknown properties based on established correlations, e.g. the derivation of the fatigue strength from tensile strength or hardness. The guideline [11] can be complemented by the guideline „Analytical strength justification with explicit consideration of nonlinear material deformation behavior" [12] which can often help to significantly increase the load margins. By considering nonlinear deformation behavior, the justification scheme often becomes less conservative. In any case, the justification according to [11] remains valid, but can be replaced by [12] to increase the performance of the part, if it results in significantly higher load margins. Finally, the FKM guideline "Fracture mechanics based strength assessment for engineering components" [13] is based on fracture mechanics and is applicable for components already containing defects or cracks when entering their service life. In recent years, several extensions of the FKM guidelines were implemented or are currently discussed which increase their range of applicability, e.g. with respect to additional material classes like high

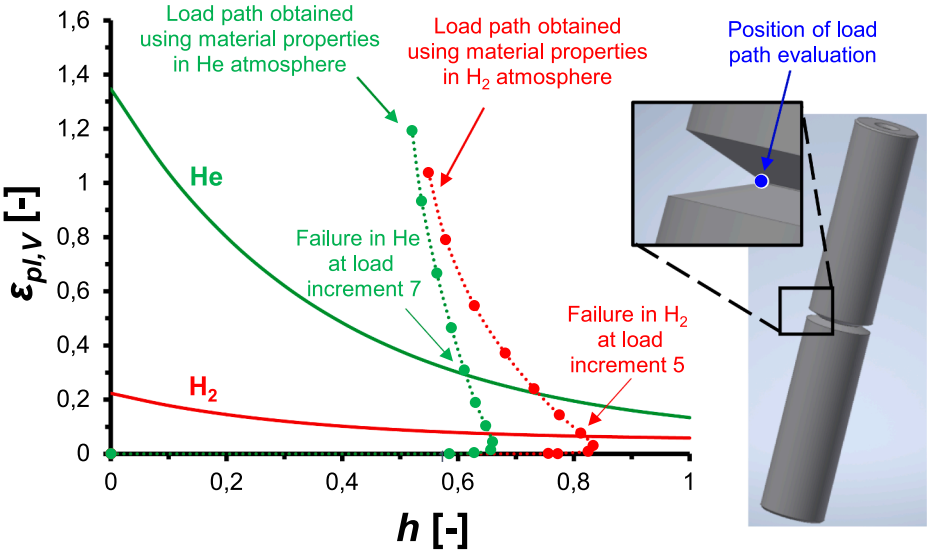

Fig. 11. Nonlinear static strength dimensioning scheme according to [12]. Exemplary failure limit curves (maximum allowable equivalent plastic strain $\varepsilon_{pl,V}$. plotted against triaxiality parameter h) for steel X3CrNiMo13-4 derived for hydrogen and helium atmosphere (continuous lines, based on data from [17]) and load paths (dashed lines) from the FE analysis of a sample component (notched tensile specimen), using stress–strain curves of hydrogen and helium atmosphere. As soon as the load path intersects with the failure limit curve, failure of the component is reached.

Table 1
Material properties ($R_{p0.2}$, R_m, A, RA) under helium (He) and hydrogen (H_2) atmosphere (both at room temperature and 10 MPa gas pressure) for steel X3CrNiMo13-4 [17] and derived parameters for the corresponding failure limit curves (ε_0, $\varepsilon_{ref,1}$, β) according to [12].

Property	Unit	He	H_2
0.2 % yield strength, $R_{p0.2}$	MPa	881	889
Ultimate tensile strength, R_m	MPa	975	966
Tensile fracture strain, A	%	21	6
Tensile uniform strain, A_g	%	8	6
Tensile reduction of area, RA	%	74	20
ε_0	%	5	5
$\varepsilon_{ref,1}$	%	135	22
β	–	2.73	3.01

strength steels [16] or copper alloys.

Hydrogen effects are not specifically addressed in the FKM guidelines in their current form. However, a future extension of the existing guidelines for hydrogen effects would be a promising way in order to provide easy to use dimensioning schemes for general engineering components under hydrogen atmosphere. Due to the important role and strong significance of the guidelines especially for SMEs, first research activities were started recently. In simple cases, the dimensioning schemes of the existing guidelines could already be applied, even if hydrogen conditions are not within their range of applicability and specific hydrogen-related damage mechanisms are not considered. Such a simple case study is demonstrated in the following.

7.2. Case study: Nonlinear strain-based static strength justification scheme accounting for degraded material properties under hydrogen atmosphere

As an example, the nonlinear strain-based static strength justification scheme according to [12] is discussed in the following, using degraded material properties under hydrogen atmosphere. The scheme is outlined in Fig. 10. By comparing the results obtained using the initial material properties (air or inert helium atmosphere) and those under hydrogen atmosphere, the reduction of the resulting load margins of the component can be evaluated. As component, a notched tensile specimen is studied in this example, which is illustrated in Fig. 11 together with the resulting failure limit curves. It needs to be emphasized that specific damage mechanisms related to the hydrogen atmosphere are not considered here and that hydrogen conditions are not within the range of applicability of the guidelines. Consequently, this study is for academic purposes only. Failure limit curves are derived for reference (air or helium) and hydrogen atmospheres according the procedure described in [12], which define the maximum allowable plastic strain before the component fails. The maximum allowable plastic strain $\varepsilon_{pl,V}$ (notation according to [12]) is plotted against the triaxiality parameter h characterizing the stress state according to Eq. (10)

$$\varepsilon_{pl,V}(h) = \varepsilon_0 + \left(\varepsilon_{ref,1} - \varepsilon_0\right) e^{-\beta h} \tag{10}$$

with $\varepsilon_{pl,V}$ being the maximum allowable plastic strain defining the failure limit curve, $h = \sigma_h/\sigma_{eq}$ the stress triaxiality parameter (ratio of hydrostatic and von Mises stress), ε_0 the minimum allowable strain given in [12] for different material classes, $\varepsilon_{ref,1}$ referring to the true fracture strain at a stress triaxiality of $h = 0$ and the exponent β as material-dependent property, defined in [12] for different material classes.

To demonstrate the hydrogen effect on the failure limit curve, exemplary material properties under hydrogen and reference conditions were implemented for the steel X3CrNiMo13-4, considering the characteristic tensile properties (0.2 % yield strength $R_{p0.2}$, ultimate tensile strength R_m, fracture strain A, reduction of area RA) given in Table 1 for helium and hydrogen atmospheres [17]. The resulting failure limit curves are plotted in Fig. 11. When comparing the curves, a strong reduction of the maximum allowable plastic strain under hydrogen atmosphere is obvious.

The load path is determined via nonlinear FE simulation of a sample component by evaluating the equivalent plastic strain and the triaxiality parameter at the hotspot of the structure at each load increment. As shown in Fig. 11, the failure of the component is reached when the load path intersects with the limit curve. As material law, isotropic von Mises plasticity is used in the FE simulations, where the stress–strain curves are derived from force–displacement curves of smooth specimens given in [17] for hydrogen and helium atmosphere. As shown in Fig. 11, there is a significant effect of the material properties on the failure limit curve and thus, the point of failure is reached significantly earlier for hydrogen conditions (load increment 5 for hydrogen and load increment 7 for helium, respectively).

This simple example demonstrates a possible concept to consider hydrogen effects in the form of degraded material properties already with the existing dimensioning schemes in [12], without specifically addressing the damage mechanisms under hydrogen atmosphere. However, this represents an academic example only and is not within the range of applicability of the current version of the FKM guidelines

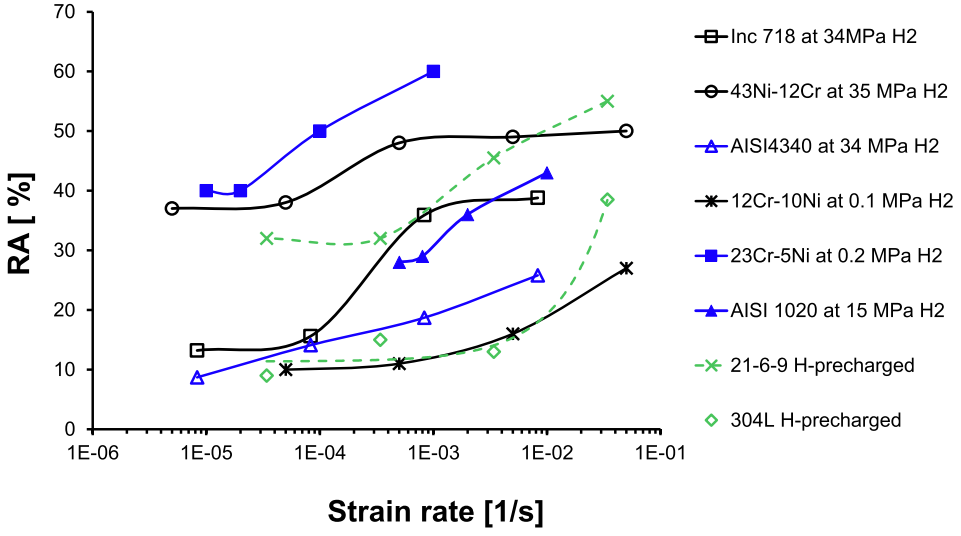

Fig. 12. Effect of strain rate on tensile reduction of area (RA) of various alloys tested in gaseous hydrogen atmosphere or pre-charged with hydrogen. Figure reproduced from [42].

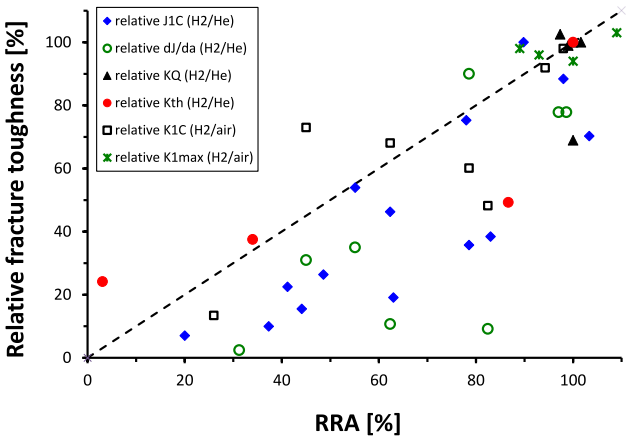

Fig. 13. Relative fracture toughness values as a function of the corresponding relative reduction of area (RRA) of smooth specimen tensile tests. The dashed line represents the one-by-one ratio. Figure reproduced from [42].

[11–13]. Significant future effort is needed to extend and to validate the FKM guidelines for systematic consideration of hydrogen effects in a general way. The existing guidelines are considered as an ideal basis for implementing such extensions due to their applicability for a vast variety of engineering components and their acceptance especially for SME.

8. Material test standards for gaseous hydrogen applications

One precondition for all above mentioned design standards for hydrogen applications are material test standards that allow the acquisition of the mechanical properties under the influence of gaseous hydrogen which are required for the design of hydrogen components. In the following, the specified test conditions of the known relevant standards are summarized and discussed.

8.1. ASTM G142 (2016)

ASTM G142 (2016) "Determination of Susceptibility of Metals to Embrittlement in Hydrogen Containing Environments at High Pressure, High Temperature, or Both" specifies quasistatic tensile testing in a gaseous hydrogen atmosphere. It provides general recommendations for both, a suitable test apparatus as well as suitable test conditions. For the hydrogen test atmosphere, ASTM G142 specifies an oxygen impurity of less than 1 ppm in hydrogen during testing since it is known that oxygen impurities as low as a few ppm can significantly influence test results [18–21]. Deviating from standard tensile testing (e.g. ASTM 8, ISO 6892-1), ASTM G142 specifies a constant extension rate of 0.002 mm/s for smooth specimens and 0.02 mm/s for notched specimens. For a typical gauge length of 30 mm for smooth specimens, this translates into a nominal strain rate of $\mathrm{d}\varepsilon/\mathrm{d}t = 6.7{\cdot}10^{-5}/\mathrm{s}$. The rationale for this requirement is the strain rate dependence of hydrogen effects in tensile tests where maximum hydrogen effects are detected at strain rates below $\mathrm{d}\varepsilon/\mathrm{d}t = 10^{-2}$ to $10^{-5}/\mathrm{s}$ depending on the material (Fig. 12).

ASTM G142 is a pure test standard, i.e. it specifies relevant test conditions but it does not provide guidance on how to use the test results for the design of hydrogen wetted components. However, ASTM G142 suggests an assessment of the materials susceptibility to hydrogen effects since it is stated that "it is common to use the ratio of the [mechanical properties] with corresponding data developed for the same material in the control test conducted in an inert gas environment at the same temperature and pressure as the hydrogen environment test. Values of these ratios near unity typically indicate high resistance to hydrogen embrittlement and lower values indicate susceptibility to embrittlement." Tensile testing is probably the most widely used method to investigate the susceptibility of alloys in gaseous hydrogen atmospheres, probably due to its simplicity. The numerous results in the open literature show that the yield strength is not affected when tensile testing in gaseous hydrogen. The ultimate tensile strength is only affected for alloys that show severe hydrogen effects. This leaves the relative elongation at fracture and the relative reduction of area as suitable hydrogen embrittlement indices to classify alloys which was successfully shown by NASA already in the 1970s [22]. It shall be emphasized here that a classification of materials based on tensile tests shall not be generalized, i.e. when a material is classified as "negligible embrittled" in tensile tests, this does not automatically mean that said material would be categorized accordingly in fatigue life tests, fatigue crack growth tests or fracture toughness tests. An example is shown in Fig. 13 where the relative fracture toughness is plotted as a function of the corresponding relative reduction of area (RRA) of smooth tensile specimens. The trend of this literature data review shows that RRA values are generally higher compared to their corresponding relative fracture toughness values.

8.2. ANSI/CSA CHMC 1 (2014)

ANSI/CSA CHMC 1 (2014) "Test methods for evaluating material compatibility in compressed hydrogen applications – Metals" provides uniform test methods for measuring material properties in gaseous hydrogen environment. The test methods include tensile testing, fracture toughness testing (K_{IH} and J_{IH}), fatigue crack growth testing (ΔK_{th}, $\mathrm{d}a/\mathrm{d}N$) and fatigue life testing (S–N)—. For all tests methods, the maximum allowable oxygen impurity of 1 ppm complies with ASTM G142 and ANSI/CSA CHMC 1 provides further information and guidance on how to obtain the required gas purity during testing.

For smooth specimen tensile tests, ANSI/CSA CHMC 1 specifies testing in constant extension rate mode which translates to a nominal strain rate of $\mathrm{d}\varepsilon/\mathrm{d}t = 10^{-5}/\mathrm{s}$. This does not exactly comply with ASTM G142 where the specified nominal strain rate is slightly higher (see Section 8.1). For notched specimens, "tests shall be conducted at applied displacement rates such that the effective strain rate measured over 25.4 mm (1 in.), centered over the notch, is nominally $10^{-6}/\mathrm{s}$ (this is one order of magnitude slower than the specified rate for the standard smooth specimen using the same test fixtures)". This is in contradiction to ASTM G142 where the extension rate of the notched specimen tensile test is one magnitude faster (0.02 mm/s) compared to the smooth specimen tensile test (0.002 mm/s). It appears desirable to align both standards upon their next revisions to avoid confusion.

For fracture toughness (K_{IH} and J_{IH}) testing, ANSI/CSA CHMC 1 recommends CTor single edge bend (SEB) specimens (dimensions according to ASTM E1820 being tested in constant displacement mode with a displacement rate between 0.1 and 1 $\mathrm{MPa}\sqrt{\mathrm{m}}/\mathrm{min}$ during the nominally elastic region of specimen loading. K_{IH} and J_{IH} testing in constant load mode is not specified in ANSI/CSA CHMC 1 although it is known that test results can differ significantly when testing with either mode, see e.g. [23].

For fatigue crack growth testing (ΔK_{th}, $\mathrm{d}a/\mathrm{d}N$), ANSI/CSA CHMC 1 allows CT specimens, middle tension (MT) specimens and eccentrically loaded single edge crack tension specimens (ESET) according to ASTM E647. The specified test parameters are a R_σ-ratio of $R_\sigma = 0.1$, a frequency of 1 Hz and a triangle or sine waveform. The rationale for a test frequency of 1 Hz is the influence of frequency on the fatigue crack growth rate. In general, the fatigue crack growth rate increases with decreasing frequency for a variety of steels [24–32] and in many cases, the effect nearly levels out at frequencies below 1 Hz [24,27,31,32]. That is, a test frequency of 1 Hz appears to be a good compromise between test duration and test result conservatism.

For load–controlled fatigue life tests (Woehler, S–N— curves), ANSI/CSA CHMC 1 allows specimens in accordance with ASTM E466. When using notched specimens, the stress concentration factor K_{t} shall be equal or greater than 3 ($K_{\mathrm{t}} \geq 3$). For strain–controlled fatigue life tests,

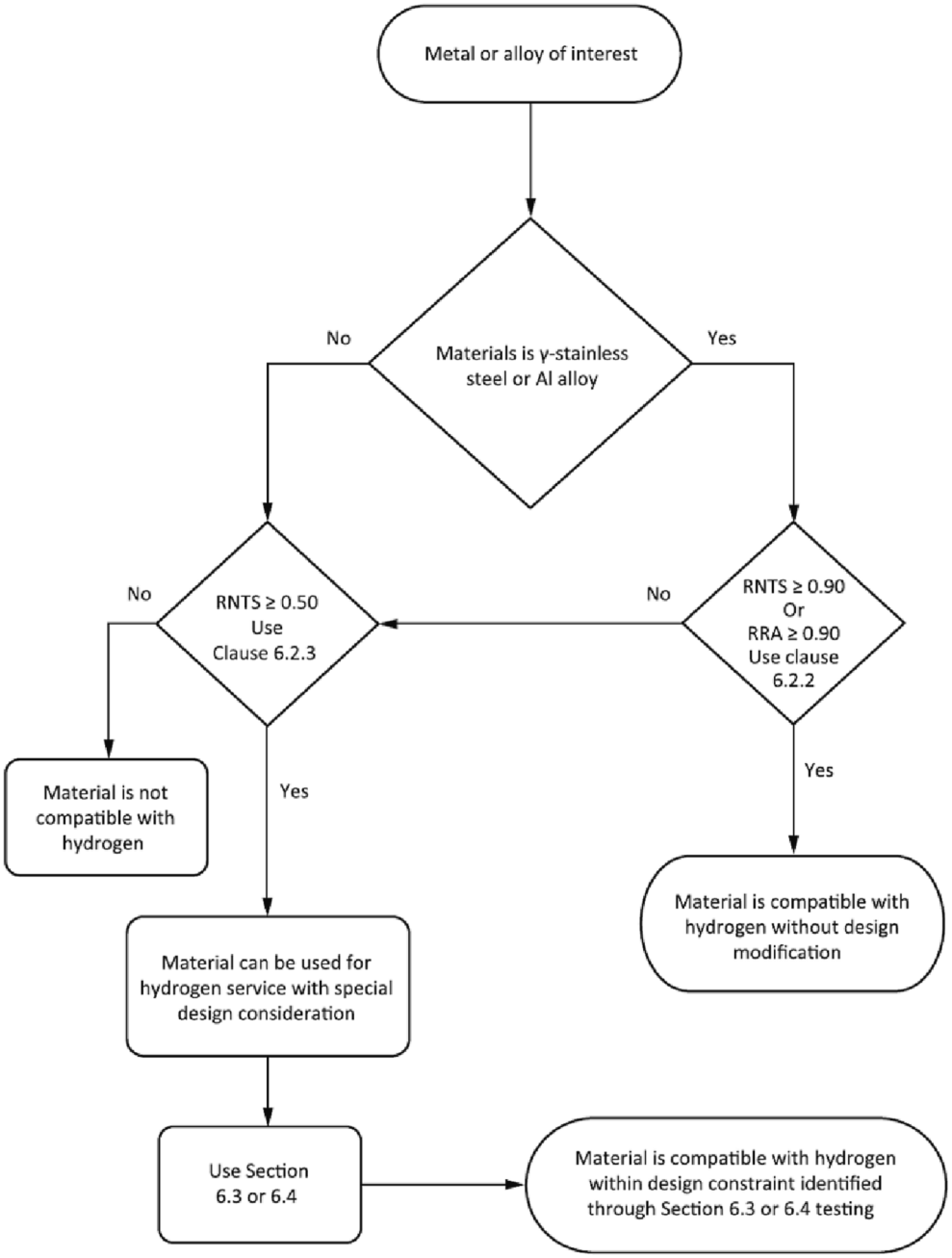

Fig. 14. Material qualification process according to ANSI/CSA CHMC 1.

ANSI/CSA CHMC 1 allows specimens in accordance with ASTM E606. The specified test parameters are *R*-ratios of 0.1 (notched specimens, load-controlled) or -1 (smooth specimens, strain-controlled), frequencies of less than 1 Hz (low cycle fatigue regime with less than 10^5 cycles) or less than 20 Hz (high cycle fatigue regime with more than 10^5 cycles) and a triangle or sine waveform. As for the fatigue crack growth tests, the same rationale for a test frequency of 1 Hz applies for the fatigue life tests.

ANSI/CSA CHMC 1 provides guidance about the selection of the appropriate test pressure and temperature. While the selection of the test pressure to be equal or greater than the maximum allowable working pressure of the component is intuitive, the selection of the appropriate test temperature is not. It is known that the deterioration of the mechanical properties of metallic materials in gaseous hydrogen atmospheres shows a maximum at a dedicated temperature (TMHE, Temperature of Maximum Hydrogen Embrittlement), which is material-dependent. It is recommended that materials testing shall be performed at TMHE or at the bounding service temperature nearest TMHE. ANSI/CSA CHMC 1 recommends testing at 220 K for austenitic stainless steels and at room temperature for nickel-based alloys and carbon and low alloy steels. These temperatures represent the average TMHE of such alloy classes [33,34] but it shall be emphasized here that this assumption shall be verified especially for carbon and low alloy steels [33,34]. For such steels and if room temperature is not the major service temperature of the component, ANSI/CSA CHMC 1 proposes to determine TMHE by notched specimens tensile testing at different temperatures.

ANSI/CSA CHMC 1 provides a methodology to qualify a material for gaseous hydrogen applications (Fig. 14). Similar to ASTM G142, ANSI/CSA CHMC 1 proposes to use relative material properties for the qualification process, i.e. the ratio of a mechanical property with corresponding data developed for the same material in a control test. A material is classified as “not compatible with hydrogen” when the

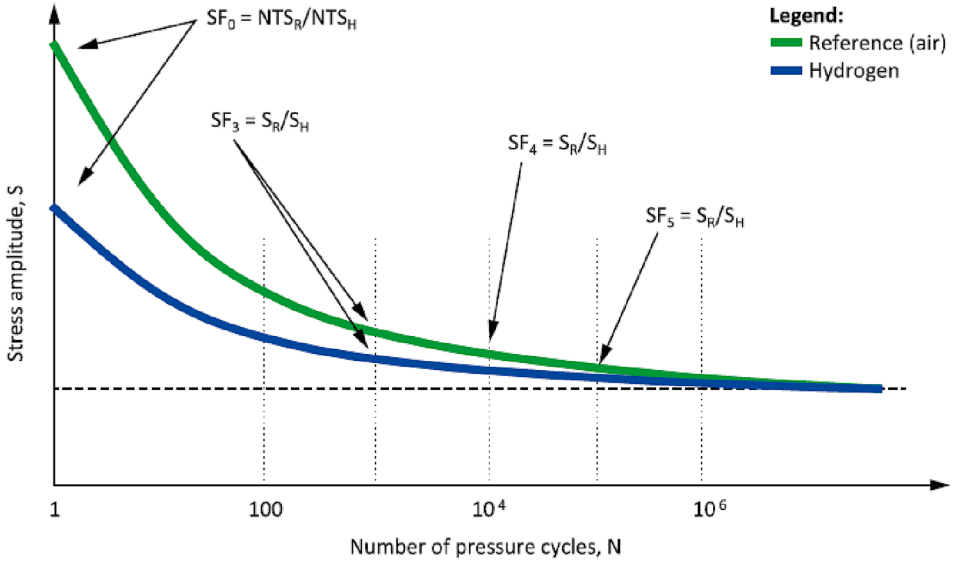

Fig. 15. Material qualification using the safety multiplier method according to ANSI/CSA CHMC 1.

relative notched tensile strength (RNTS) is less than 0.5 (RNTS less than 0.5). A rationale for this boundary could not be identified and there might be applications where materials with RNTS less than 0.5 can be safely used in hydrogen applications, e.g. for unloaded or very low loaded parts. On the other hand, a material is classified as "compatible with hydrogen" when RNTS $\geq$ 0.9 or RRA $\geq$ 0.9. As mentioned in Section 8.1 discussing ASTM G142, this assessment from tensile testing cannot be generalized, i.e. when a material is classified as "compatible with hydrogen" in tensile tests, this does not automatically mean that said material would be categorized accordingly in fatigue life tests, fatigue crack growth tests or fracture toughness tests (Fig. 13).

From an engineering point of view, probably the most relevant method is the determination of a hydrogen safety factor. ANSI/CSA CHMC 1 outlines the determination of a hydrogen safety factor by load-controlled fatigue life testing in the low cycle fatigue regime using notched specimens. In short, based on a statistical analysis of experimental data, four safety factors (SF) are calculated at 1, 10^3, 10^4 and 10^5 cycles as $SF = S_R/S_H$, where S_R is the fatigue strength in reference atmosphere and S_H is the fatigue strength in hydrogen (Fig. 15). The hydrogen safety factor is the largest of the four ratios. This method was critically reviewed in [35] with the conclusion that the resulting hydrogen safety factor can be as high as 3 and, thus, be overly conservative. However, as mentioned before, the German AD 2000 code requires an additional safety factor of 10 for hydrogen applications, which justifies the method outlined in ANSI/CSA CHMC 1 for a design of more efficient components.

It has been shown experimentally that fatigue life curves of numerous alloys measured in reference and hydrogen atmosphere converge in the vicinity of the theoretical infinite life, i.e. at about $2{\cdot}10^6$ cycles [36–41] . That is, the sketch shown in Fig. 15 appears to visualize a realistic trend in a way that performing time consuming and costly tests at low loads to determine the fatigue strength at 10^4 and 10^5 cycles might not be necessary. This leaves the comparison of SF_0 = RNTS (1 cycle) and SF_3 (10^3 cycles). This might be worth discussing at the next revision of ANSI/CSA CHMC 1.

8.3. ISO 11114-4 (2017)

ISO 11114-4 (2017) "Transportable gas cylinders — Compatibility of cylinder and valve materials with gas contents — Part 4: Test methods for selecting steels resistant to hydrogen embrittlement" specifies material test methods and material qualification metrics for transportable seamless steel gas cylinders at pressures greater than 5 MPa. Since this standard is the only ISO standard in this field, it is often misquoted as a standard to determine hydrogen susceptibility in general. It shall be emphasized here, that ISO 11114-4 should not be used for other applications without a careful consideration of the requirements of the other application. The following review focusses on the test methods described in ISO 11114-4. For all tests methods, the maximum allowable oxygen impurity is 1 ppm (and less than 3 ppm H_2O), which complies with ASTM G142 and ANSI/CSA CHMC 1.

Method A describes a disk test where a disk (diameter 58 mm, thickness 0.75 mm) is biaxially deformed by a hydrogen gas pressure until rupture. The result is a burst pressure in hydrogen, which is compared with a burst pressure in an inert control gas. A steel is qualified for the given application when the ratio of the burst pressures in hydrogen and control gas is greater than two. This test does not provide basic material properties. However, quantifying the plastic deformation by using e.g. digital image correlation would yield a biaxial stress stain curve, which can be very helpful when designing pressure components.

Method B describes the determination of the fracture toughness in hydrogen (K_{IH}) in a step load test using CT specimens. Starting with a defined pre-crack the specimen shall be loaded with a stress intensity factor of 1 MPa$\sqrt{\text{m}}$ at the crack tip and be held for 20 min. If no crack growth is detected by the end of the hold period, the load shall be increased in a defined way and held for another 20 min. This procedure shall be continued until fracture occurs. Finally, K_{IH} is calculated following ISO 7539-6. If K_{IH} is equal or greater than 60/950 UTS in MPa$\sqrt{\text{m}}$, the material is qualified up to this ultimate tensile strength (UTS). A rationale for this qualification requirement could not be found, especially for the factor 60/950, which implies that it is specific for the given application and might not be transferred to other applications

without a careful assessment.

Method C describes the determination of a stress intensity in hydrogen (K_{arrest}) in a constant displacement test using CT specimens. Starting with a defined pre–crack, the specimen shall be loaded with a defined displacement rate (V) up to a defined stress intensity factor K_{IAPP}. At K_{IAPP}, the crack grows until the stress intensity reaches a lower bound where the crack arrests (K_{arrest}). Formulas for both, V and K_{IAPP} are given in ISO 11114-4. The steel is qualified up to its UTS when i) the measured crack growth does not exceed 0.25 mm or ii) the measured crack growth exceeds 0.25 mm and K_{arrest} is equal or greater than 60/950 UTS in MPa$\sqrt{m}$. Again, this method appears to create specific data for the qualification of steels for the given application and does not provide basic material properties. That is, this qualification requirement also appears specific for the given application and might not be transferred to other applications without a careful assessment.

9. Summary and conclusions

The results can be summarized as follows:

For the assessment of existing pipelines that shall be re-qualified from natural gas to hydrogen transport, the fracture mechanics design approach of the ASME B31.12 is the only approach currently in existence. Several options to reduce the conservatism of the current version of the ASME B31.12 code are proposed, e.g. by a careful analysis of the initial crack aspect ratio and initial crack depth as well as by selecting the appropriate stress intensity factor solution and fatigue crack growth law. For the design of new storage tanks and other components, the fatigue-based approach should also be considered for the assessment of the influence of gaseous hydrogen. The German AD 2000 code proposes a methodology based on a fatigue life approach. However, the current version of the AD 2000 code also provides several options to reduce the conservatism, i.e. by accounting for the influence of the hydrogen gas pressure, the influence of the load cycle frequency and the load ratio, the influence of the microstructure morphology in terms of the weld seam with base material, weld material and heat affected zones and the influence of the temperature. In addition the German FKM guidelines provide a framework for additional design options, which is subject to current development.

All relevant material test methods are specified in ANSI/CSA CHMC 1. However, detailed test conditions are not harmonized with other existing test standards, e. g. ASTM G142 or ISO 11114-4 (Table 2). It is suggested that this might be harmonized in the next revisions of the respective standards to avoid confusion.

Table 2
Codes and standards for material tests in gaseous hydrogen. * only constant displacement mode, ** only step load mode and constant displacement mode for K_{arrest}.

Tensile test	Fatigue life test (Woehler)	Fatigue crack growth test (da/dN)	Fracture toughness test (K_{IH}, J_{IH})
• ANSI/CSA CHMC 1 • ASTM G142	ANSI/CSA CHMC 1	ANSI/CSA CHMC 1	• ANSI/CSA CHMC 1* • ISO 11114-4**

Declaration of Competing Interest

The authors declare the following financial interests/personal relationships which may be considered as potential competing interests: [Thorsten Michler reports financial support was provided by German Federal Ministry for Economic Affairs and Climate Action (BMWK) under grant numbers 03HY202F (TransHyDE) and 03HY301F (H2Mare).].

Data availability

Data will be made available on request.

Acknowledgements

This study was financially supported by the German Federal Ministry for Economic Affairs and Climate Action (BMWK) under grant numbers 03HY202F (TransHyDE) and 03HY301F (H2Mare).

References

[1] S.P. Lynch, Hydrogen embrittlement (HE) phenomena and mechanisms, in: V.S. Raja, T. Shoji (Eds.), Stress Corros. Crack. Theory Pract., Woodhead Publishing, 2011: pp. 90–130. https://doi.org/10.1533/9780857093769.1.90.
[2] Oriani RA. A mechanistic theory of hydrogen embrittlement in steels. Berichte Der Bunsengesellschaft 1972;76:848–57.
[3] Birnbaum HK, Sofronis P. Hydrogen-enhanced localized plasticity—a mechanism for hydrogen-related fracture. Mater Sci Eng A 1994;176:191–202. https://doi.org/10.1016/0921-5093(94)90975-X.
[4] Amaro RL, White RM, Looney CP, Drexler ES, Slifka AJ. Development of a Model for Hydrogen-Assisted Fatigue Crack Growth of Pipeline Steel1. J Press Vessel Technol Trans ASME 2018;140:1–13. https://doi.org/10.1115/1.4038824.
[5] Slifka AJ, Drexler ES, Amaro RL, Hayden LE, Stalheim DG, Lauria DS, et al. Fatigue Measurement of Pipeline Steels for the Application of Transporting Gaseous Hydrogen. J Press Vessel Technol 2018;140:581–92. https://doi.org/10.1115/1.4038594.
[6] A.J. Slifka, E.S. Drexler, N. Rustagi, D.S. Lauria, J.D. McColskey, R.L. Amaro, A.E. Stevenson, P.G. Keefe, Fatigue crack growth of two X52 pipeline steels in a pressurized hydrogen environment, in: B.P. Somerday, P. Sofronis (Eds.), Proc. 2012 Int. Hydrog. Conf. Hydrog. Mater. Interact. 9-12 Sept 2012, ASME Press, Jackson Lake Lodge, WY, USA, 2012: pp. 299–308.
[7] Drexler ES, Slifka AJ, Amaro RL, Barbosa N, Lauria DS, Hayden LE, et al. Fatigue crack growth rates of API X70 pipeline steel in a pressurized hydrogen gas environment. Fatigue Fract Eng Mater Struct 2014;37:517–25. https://doi.org/10.1111/ffe.12133.
[8] C. San Marchi, J. Ronevich, P. Bortot, Y. Wada, J. Felbaum, M. Rana, Technical basis for master curve for fatigue crack growth of ferritic steels in high pressure gaseous hydrogen in ASME Section VIII-3 code, in: Proc. ASME 2019 Press. Vessel. Pip. Conf. (PVP2019), 14-19July2019, ASME Press, San Antonio, TX, USA, 2019: p. PVP 2019-93907.
[9] Michler T, Wackermann K, Schweizer F. Review and Assessment of the Effect of Hydrogen Gas Pressure on the Embrittlement of Steels in Gaseous Hydrogen Environment. Metals (Basel) 2021;11:637. https://doi.org/10.3390/met11040637.
[10] Ronevich JA, Song EJ, Somerday BP, San Marchi CW. Hydrogen-assisted fracture resistance of pipeline welds in gaseous hydrogen. Int J Hydrogen Energy 2021;46:7601–14. https://doi.org/10.1016/j.ijhydene.2020.11.239.
[11] Rennert R, Kullig E, Vormwald M, Esderts A, Luke M. Analytical strength justification for engineering components, 7th eds. Frankfurt am Main, Germany: VDMA-Verlag; 2020.
[12] Fiedler M, Wächter M, Varfolomeev I, Vormwald M, Esderts A. Analytical strength justification with explicit consideration of nonlinear material deformation behavior, 1st eds. Frankfurt am Main, Germany: VDMA-Verlag; 2019.
[13] Berger C, Blauel J, Hodulak L, Pyttel B, Varfolomeev I. Fracture mechanics based strength assessment for engineering components, 4th eds. Frankfurt am Main, Germany: VDMA-Verlag; 2018.
[14] www.fkm-net.de, (n.d.).
[15] www.vdma.org, (n.d.).

[16] T. Straub, I. Varfolomeev, M. Luke, A. Kleemann, S. Kleemann, T. Richter, H. Beinersdorf, P. Yadegari, T. Beier, M. Vormwald, Entwicklung einer validierten Methodik zur Berechnung der Schwingfestigkeit von Bauteilen aus höchstfesten Stählen (in German), in: FKM-Vorhaben Nr. 610, H. 340, VDMA-Verlag, Frankfurt am Main, Germany, 2021: p. 218.
[17] Deimel P, Sattler E. Untersuchungen zum Wasserstoffeinfluss auf im Kompressorbau eingesetzte Werkstoffe (in German). Frankfurt am Main, Germany: Forschungskuratorium Maschinenbau; 2007.
[18] Michler T, Boitsov IE, Malkov IL, Yukhimchuk AA, Naumann J. Assessing the effect of low oxygen concentrations in gaseous hydrogen embrittlement of DIN 1.4301 and 1.1200 steels at high gas pressures. Corros Sci 2012;65:169–77. https://doi.org/10.1016/j.corsci.2012.08.015.
[19] J. Ronevich, C. San Marchi, R. Kolasinski, K. Thurmer, N. Bartelt, F. El Gabaly, B. Somerday, Oxygen Impurity Effects on Hydrogen Assisted Fatigue and Fracture of X100 Pipeline Steel, in: Proc. ASME 2018 Press. Vessel. Pip. Conf. (PVP 2018), 15-20July2018, American Society of Mechanical Engineers, Prague, Czech Republic, 2018: pp. PVP2018-84163. https://doi.org/10.1115/PVP2018-84163.
[20] Somerday BP, Sofronis P, Nibur KA, San Marchi C, Kirchheim R. Elucidating the variables affecting accelerated fatigue crack growth of steels in hydrogen gas with low oxygen concentrations. Acta Mater 2013;61:6153–70. https://doi.org/10.1016/j.actamat.2013.07.001.
[21] Komoda R, Kubota M, Staykov A, Ginet P, Barbier F, Furtado J. Inhibitory effect of oxygen on hydrogen-induced fracture of A333 pipe steel. Fatigue Fract Eng Mater Struct 2019;42:1387–401. https://doi.org/10.1111/ffe.12994.
[22] R.P. Jewett, R.J. Walter, W.T. Chandler, R.P. Frohmberg, Hydrogen Environment Embrittlement of Metals, in: NASA-CR-2163, National Aeronautics and Space Administration, 1973: p. 238.
[23] K.A. Nibur, B.P. Somerday, C.W. San Marchi, J.W. Foulk, M. Dadfarnia, P. Sofronis, G.A. Hayden, Measurement and interpretation of threshold stress intensity factors for steels in high-pressure hydrogen gas, Livermore, CA, USA, 2010.
[24] Suresh S, Ritchie RO, Suresh DRO. Mechanistic dissimilarities between environmentally influenced fatigue-crack propagation at near-threshold and higher growth rates in lower strength steels. Met Sci 1982;16:529–38.
[25] Lo SH, Johnson HH. Fatigue of, steel in hydrogen. Scr Metall 2018;20(1986): 85–180.
[26] Y. Murakami, T. Kanezaki, Y. Mine, S. Matsuoka, Hydrogen embrittlement mechanism in fatigue of austenitic stainless steels, Metall. Mater. Trans. A Phys. Metall. Mater. Sci. 39 A (2008) 1327–1339. https://doi.org/10.1007/s11661-008-9506-5.
[27] M. Yoshikawa, N. Tsutsumi, S. Matsuoka, Y. Murakami, Effect of test frequency and hydrogen pressure on crack growth of a ferrite-pearlite steel in hydrogen gas, in: Proc. 29th Symp. Fatigue, The Society of Materials Science, Japan. JSMS Committee on Fatigue of Materials, n.d.: pp. 120–123.
[28] Kotake H, Matsumoto R, Taketomi S, Miyazaki N. Transient hydrogen diffusion analyses coupled with crack-tip plasticity under cyclic loading. Int J Press Vessel Pip 2008;85:540–9. https://doi.org/10.1016/j.ijpvp.2008.02.002.
[29] Smith P, Stewart AT. Effect of aqueous and hydrogen environments on fatigue crack growth in 2Ni-Cr-Mo-V rotor steel. Met Sci 1979;7:429–35.
[30] Tanaka H, Homma N, Matsuoka S, Murakami Y. Effect of hydrogen and frequency on fatigue behaviour of SCM435 steel for storage cylinder of hydrogen station. Trans Japan Soc Mech Eng A 2007;73:1358–65.
[31] A.H. Priest, Fatigue crack growth and fracture resistance of steels in high-pressure hydrogen environments, in: EHC-(1)42-012-81 UK(H), Commission of the European Communities, Directorate-General Science, Research and Development, Luxemburg, 1983: p. 67.
[32] Yamabe J, Yoshikawa M, Matsunaga H, Matsuoka S. Effects of hydrogen pressure, test frequency and test temperature on fatigue crack growth properties of low-carbon steel in gaseous hydrogen. Procedia Struct Integr 2016;2:525–32. https://doi.org/10.1016/j.prostr.2016.06.068.
[33] Michler T, Schweizer F, Wackermann K. Review on the Influence of Temperature upon Hydrogen Effects in Structural Alloys. Metals (Basel) 2021;11:423–38.
[34] T. Michler, K. Wackermann, F. Schweizer, Correction: Michler et al. Review and Assessment of the Effect of Hydrogen Gas Pressure on the Embrittlement of Steels in Gaseous Hydrogen Environment. Metals 2021, 11, 637, Metals (Basel). 11 (2021) 637.
[35] Yamabe J, Matsunaga H, Furuya Y, Hamada S, Itoga H, Yoshikawa M, et al. Qualification of chromium-molybdenum steel based on the safety factor multiplier method in CHMC1-2014. Int J Hydrogen Energy 2015;40:719–28. https://doi.org/10.1016/j.ijhydene.2014.10.114.
[36] Schauer G, Roetting J, Hahn M, Schreijaeg S, Bacher-Höchst M, Weihe S. Influence of Gaseous Hydrogen on Fatigue Behavior of Ferritic Stainless Steel - A Fatigue-life Estimation, in. Procedia Eng, Elsevier Ltd 2015:362–78. https://doi.org/10.1016/j.proeng.2015.12.669.
[37] Balitskii A, Vytvytskyii V, Ivaskevich L, Eliasz J. The high- and low-cycle fatigue behavior of Ni-contain steels and Ni-alloys in high pressure hydrogen. Int J Fatigue 2012;39:32–7. https://doi.org/10.1016/j.ijfatigue.2011.05.017.
[38] Aoki Y, Kawamoto K, Oda Y, Noguchi H, Higashida K. Fatigue characteristics of a type 304 austenitic stainless steel in hydrogen gas environment. Int J Fract 2005; 133:277–88. https://doi.org/10.1007/s10704-005-4942-3.
[39] Fukuyama S, Yokogawa K, Kudo K, Araki M. Fatigue properties of type 304 stainless steel in high pressure hydrogen at room temperature. Trans Japan Inst Met 1985;26:325–31.
[40] Fujino Y, Kawabe N, Izumida H. Development of highly hydrogen-resistant stainless steel spring wire. SEI Tech Rev 2006:60–4.
[41] Tkachev VI, Vytvyts'kyi VI, Hrebenyuk SO. Multicycle fatigue of steels in hydrogen under high pressures. Mater Sci 1998;34:122–4.
[42] Michler T, Lindner M, Eberle U, Meusinger J. Assessing hydrogen embrittlement in automotive hydrogen tanks. In: Gangloff RP, Somerday BP, editors. Gaseous Hydrog. Embrittlement Mater. Energy Technol. Oxford, Cambridge, Philadelphia, New Dheli: Woodhead Publishing; 2012. p. 94–125. https://doi.org/10.1533/9780857093899.1.94.